Conceptual Design, and Fluid-Structural Interaction Based Investigations on Highly Maneuverable Unmanned Amphibious Vehicle for Ravage Removal Applications at Various Oceanic Working Environments

Senthil Kumar Madasamy
Kumaraguru College of Technology
Vijayanandh Raja (vijayanandh.raja@gmail.com)
Kumaraguru College of Technology https://orcid.org/0000-0003-4992-3028
Sangeetha Ganesan
Kumaraguru College of Technology
Dharshini Murugan
Kumaraguru College of Technology
Arul Prakash Raji
Kumaraguru College of Technology
Darshan Kumar Jayaram
Kumaraguru College of Technology

Research Article

Keywords: Aerodynamics, Alloys, Composite Materials, CFD, Ravage removal, Hydro structural, Hydrodynamics, Tropic Bird.

Posted Date: September 1st, 2021

DOI: https://doi.org/10.21203/rs.3.rs-774147/v1

Conceptual Design, and Fluid-Structural Interaction based Investigations on Highly Maneuverable Unmanned Amphibious Vehicle for Ravage Removal Applications at Various Oceanic Working Environments

Senthil Kumar Madasamy[1], Vijayanandh Raja[1,*], Sangeetha Ganesan[1], Dharshini Murugan[1], Arul Prakash Raji[1], Darshan Kumar Jayaram[1]

[1]Department of Aeronautical Engineering, Kumaraguru College of Technology, Coimbatore, Tamil Nadu, India

* Corresponding author: vijayanandh.raja@gmail.com

Abstract

Nowadays Unmanned Amphibious Vehicles [UAVs] are employed in many applications such as oceanic research, deep sea exploration, mapping, naval surveillance, and disaster monitoring and fisheries protection. The use of UAVs in military and other applications has steadily increased over the few years. On the other hand, there has been a tremendous increase in ocean exploitation. Though technologies are increasing incrementally, nature is exploited adversely. Advancement in ocean transportation, shipping, sewage wastes filled the ocean with tonnes and tonnes of debris and oil wastes. This ravage fills affect the complete marine ecosystem. This in turn makes the ocean toxic. Advancements have been made in recent years to clean up the oil spills. The noted projects such as Sea bin, super high-tech sponges etc. All these innovations are the static one which cannot move along the waves of the ocean. The static form of these inventions could not be used to clean to the larger extent. Therefore, this study aims to build an UAV which is a movable one, can detect the debris and clean those by incorporating existing cleaning techniques. Since the UAV has to sub merge under the water to some extent, it should be designed in such a way by considering both the hydro-dynamical and hydro structural aspects of it. The unique point in the paper covers the flexible cum efficient design of the UAV. The design of the tropical bird is chosen for the efficient model of the UAV. With the few known parameters of this species, the UAV has been designed to achieve the maximum efficiency. The tropical bird chosen has the higher rate of climb, which is the desired requirement for this study. The propeller is uniquely designed based on aerodynamic cum hydrodynamic data so as to balance both the effects. With the design data estimated using analytical formulae, the UAV has been constructed. Following the design, the complete analyses on aerodynamic, aero-structural, hydrodynamic and hydro structural computations are completed. Finally, the employment techniques such as ravage removal mechanism, integrated rotor for the selected application will be integrated. CATIA and ANSYS Workbench are the major tools involved in these comparative investigations, in which modelling of UAV is computed in CATIA and fluid pressure, structural deformations, stresses on UAV are computed through ANSYS Workbench.

Keywords: Aerodynamics; Alloys; Composite Materials; CFD; Ravage removal; Hydro structural; Hydrodynamics; Tropic Bird;

I. INTRODUCTION

Maritime transport has emerged everywhere due to its flexible, huge, and low-cost platforms. Because of this huge implementation, the sea wastes such as oil spills and aquatic debris from the major threat to the marine ecosystem. There is no such permanent solution for cleaning up the ocean from these threats. This work brought up the idea to resolve such conditions by means of ravage removal with the help of UAV. UAV is a kind of unmanned vehicle, in which the pilot need not be taking place inside the vehicle. Instead of an on board position, through the help of remote control or program control, the UAV can be engaged at the execution of the mission. This work on UAV deals with the major analysis on Aerodynamic, Aero-structural, Hydrodynamics and Hydro structural studies [Agus Budiyono (2009)].

Unmanned Amphibious vehicle is an aircraft that operated remotely by humans or autonomously by on board computers, this type of vehicle which can fly/swim both in Air and water. i.e., it can also be operated on the surface of the water to ocean depths and come back. UAV lighter than air is lifted buoyancy and heavier than air has relation motion against aerodynamics, up thrusts powered lift with engine thrust or electric power. Powered lift is produced by directing the engine thrust vertically downwards. UAV is classified into three types are seaplane UAV, submarine launched UAV and submersible UAV. Overall, aquatic UAV use electric power or hybrid powered propulsive system. Seaplane UAVs follows aerodynamics and hydrodynamics principles, but submarine launched UAV and submersible UAV working only under Hydrodynamics law, design should always decrease the drag& increase the Hydrodynamics stability. Wing Configuration of aquatic UAV is fixed wings, morphing wings, variable wings and Quadcopter. Fixed wing UAV can take off and land on water but cannot dive in. This fixed wing UAV is navigated through sea wave mode and flying mode. While in sea wave mode engine will be shutdown. This type of wing maintains neutral buoyancy in water at the same time it reduces vehicles weight. Because of lifting surface, it could achieve greater endurance. Example - flying fish is air to water transition wing an electric motor and single propeller. Morphing wing can fold its wing to increase underwater manoeuvrability [Chenhui Han et al (2019)]. Quadcopter aquatic UAV generates lift through the rotations of rotors, it is easy to enter and exit water. This type of rotor can be highly stable and good in manoeuvring, but it has less efficient and less battery life. Variable wing's structure includes folded swept wings and bio-inspired flapping wings; they can reduce frictions and improve moving efficiency. In Flapping wing UAV, most of this type of UAV is inspired by bionics. A jelly fish aquatic UAV inspired flapping wing concept. Flapping wing is efficient only for small UAV. Some applications of aquatic UAV are to measure elements such as reflection of light, research about the presence of microscopic life, under ice working- observe the creature and inspects under ice situation, water sampling and deep-sea sampling, ocean oil pipes transportations, study on diffusion, acoustic transmission, and submarine wakes. From various study, fixed wing configuration can be operated on the surface of water and underwater. This wing type is lift producing component and stable on the sea surface. This work extracted the design from white tropic bird; the bird has high stability and lift consideration. In aerodynamics perspective the authors will be using double tapered wing and in

hydrodynamics perspective the authors use linear tapered wing with attached aerodynamics rotor or propeller to reduce buoyancy and give less forward speed [Daniele Costa et al (2018)].

1.1 Aim

The predominant aim of this work is to construct the conceptual design of an UAV and thereby analyse the working condition according to the mission requirements. The work mainly focuses on design i.e., flexible and efficient design. The mission of this work is to remove Ravage and debris on the water surface and under the surface of the sea for further development. The work on this field of analysis will definitely invite new trends and technology in the air-water ecosystems.

II. LITERATURE SURVEY

Paper (Dylan K Wainwright et al 2020) dealt about the shape of living fish tuna's performance, three kinds of motion models were put forward based on the observation of fish performance and hydrodynamic performance were analysed. The methodologies used were the study about tuna fish shape, coordinates and mathematical form for motion model were derived, compared the three kinds of motion model, and analysed the hydrodynamic performance of fish for different kinematic models. The shape of tuna was taken as the bionic object to establish motion model. The study about its performance was done and analysed the high-speed photographic images of the steady-state swimming of live fish. Through analysis the spline curve characteristics were studied. The bionic motion models can be divided into Oscillating Model obeying Polynomial function (OMP), Undulatory Model obeying Polynomial function (UMP) and Undulatory Model obeying Exponential function (UME). And finally, hydrodynamic coefficients with different motion frequency and amplitude were compared. The main observations are how the comparisons are done, and the detailed study of the fish.

Paper (Meliha Bozkurttas et al 2008) dealt about the sunfish's fin, its mechanical design, motions and performance of prototype cupping fin. The methodologies used were detail study about the sunfish's fin, and the model were analysed through CFD, scaling effect of fish fin were analysed, and finally prototype of fin were analysed. First Study about the sunfish's fin was done and appropriately borrowing the crucial features of its mechanical design and motions for model. For prototype a bio-robotic fin propulsor was developed. The effect of fin kinematics on superior hydrodynamic performance of the fish fin has been analysed. Bio-robotic fins have been designed to replicate Mode-1 movement of sunfish's fin using a close plan form to the fish fin. The outcome was prototype successfully produced thrust during both the fin's outstroke and in-stroke. The further process of this paper was to study about these robotic fins to improve thrust production and control of propulsion and manoeuvring forces. The observations are how the analysis is done by CFD and major consideration characteristic when making prototype.

Paper (Negrello, F et al 2016) deals with the preliminary design of a biologically inspired flapping UAV, i.e., the aerodynamic performance and flight stability of a bio mimetic flapping UAV designed at minimum flight velocity. The methodologies used were extensive study in order to dissect the kinematics of the wings, numerical study of the avian model in terms of the aerodynamic performance and flight stability in flapping and gliding

conditions. The design specifications and morphometrics/allometry of several birds to determine the initial form of the avian model. One important design specification to highlight is that the vehicle is intended to be hand launched with a minimum velocity of 5.0 m/s. The avian model is treated as a rigid body to simplify the equations that describe the dynamics. For the flapping flight simulations, the wings are considered to be made of two parts, one internal wing and one external wing. In aerodynamic performance in gliding the unsteady incompressible Reynolds-Averaged Navier-Stokes (RANS) equations are solved by using the commercial finite volume solver Ansys. This results in a total variation diminishing (TVD) scheme that guarantees the accuracy, stability and boundedness of the solution. The pressure-velocity coupling is achieved by means of the PISO algorithm and as the solution takes place in collocated meshes. The lift force L and drag force D are calculated by integrating the pressure and wall-shear stresses over the surface of the avian model. For computing the static stability, the position of the centre of gravity CG about which the moment is computed is defined. For the design and the wide range of velocities, pitch angles and tail deflection angles were studied; it was found that the avian model and kinematics proposed were able to fulfil the design requirements. It also found that for the tail sizing and tail deflection angles considered the model has positive stability.

Paper (Xiao-xu DU et al 2014) deals with the mathematical model of UAV moving close to sea bottom was established based on the incompressible viscous flow. The structured grid of the computational models with different distances to the sea bottom and attack angles is generated by Ansys ICEM, and the flow field near the sea bottom is simulated using CFXBystron and Anderson made a model test with the vertical force and trimming moment. Kuang Xiao-feng studied the attraction characteristics of submarine sailing close to the sea bottom. Zhu Xin-yao studied the hydrodynamic characteristics of UAV parking on the seabed. Zhu Ai-jun carried out experimental study about the relationship between the drag of underwater vehicles and the distance to the sea bottom. There are mainly three methods to calculate hydrodynamic parameters 1) empirical formula2) model test 3) numerical simulation. Then numerical simulation was carried out by CFX, and the relationship among drag, lift, pitching moment features and the distance to sea bottom, attack angle was studied. For Mathematical Model to solve viscous flow problems Navier Stokes equations are used. In this paper, the RANS equations and (SST) model are used for steady incompressible flow Equation of Motion (N-S Equation) were used. For numerical study, calculation domain is formed by constructing virtual boundary. Hexahedral domain calculation is used for stimulation. The structured grid of the computational models at different distances from the sea bottom and different attack angles was generated by Ansys ICEM.

The paper (Tae-Hwan Joung et al 2006) deals with the structural design and analysis of deep sea UAV. Here the structural design and analysis of remotely operated vehicle and launcher systems were discussed having adopted the optimizing process. The launcher frames in this project were made of galvanized steel and the remotely operated vehicle made of aluminium 60 series. Since the launcher was considered as an underwater base for the operation of ROV, it has a very important role to play in the working system to reduce the impact loads. Hence galvanized steel with appropriately selected gravity is used. On the other hand, ROV has to be designed in such a way for easy operation, so aluminium 60 series which have light and corrosive resistive characteristics were used. The Structural safety of frames here are valued based on the material's yield stress, taking into account the factors for live load, loss

of strength due to welding and unexpected impact causing unusual loading. Since the regular responses like displacement and stress are not satisfying there is a need to reduce the weight of the launcher and ROV. This can be done by the optimum design process. The structural analysis was carried out using the finite element method. Based on the above said analysis the weight of the launcher and the remotely operated vehicle were reduced according to the safety factor and stress obtained. The safety factor for the maximum stress for the optimum design is about 8. From the paper it is found that the Ti alloy and Al alloy are considered as the suitable material for the pressure vessel for the UAV. Material properties such as poison's ratio, yielding stress, and ultimate stress are used to analyse the pressure vessel. Buckling dominates the collapse of pressure vessel's cylindrical part. Thus, the structures are redesigned based on the structural safety criteria.

Paper (Joon-Young Kim et al 2011) describes the dynamic modeling, structural analysis, implementation and experimental test of a Manta-type Unmanned Underwater Vehicle (MUUV). They have attempted a dynamic performance analysis and controller design using a mathematical model of the MUUV and have made experimental tests for comparison with simulation results. The mathematical model of the underwater vehicle is comprised of a vehicle body, thrusters and control surfaces. Structural analysis of MUUV is achieved by the commercial finite element analysis program, ANSYS V13.0. The MUUV needs a robust control system because the vehicle operates in rough ocean environments and the vehicle needs to return to the submarine autonomously after the mission is completed. To verify the depth and heading control simulation, free running tests were carried out in a towing tank. The paper provides an idea for structure analysis, and the methods of simulations.

2.1 Summary

Based on Literature Survey and Historical relationship, the link between payload weights to overall take-off weight of UAV is to be derived. Thus, the overall take-off weight of UAV to be calculated for other components' selection. With the help of conventional cum standard formulae, the UAVs design parameters need is completed. The modeling tool, CATIA is planned to use the construction of UAV's conceptual design. ANSYS Fluent and ANSYS Structural tools are planned to utilize to execute the Hydro-Structural Interactional Analyses. This work executes the combination process of a new platform with conventional existing techniques, wherein the new proposed platform is UAV and the conventional existing techniques such as sea bin, etc. Therefore, the final UAV's design includes the cleaner, which defines the equipment to clean up the mass. Ravage or other kinds of wastages' prediction is a very important one so this needs to be investigated carefully in order to attain a unique and good ravage removal system.

III. PROPOSED DESIGN – TROPIC BIRD INSPIRED UAV

The conceptual design of UAV was taken from the literature survey about existing species. The outer body of this proposed UAV design was captured from Tropic Bird. The major fundamental requirement of this recommended UAV must have high stability to execute the mission without any disturbances, high manoeuvring capacity to execute the sudden altitude variations with payload. The aforementioned two factors made the design of this proposed UAV complicated, so this work picked one of the perfect nature-based designs, which is Tropicbird

[Yung-Lien Wang et al (2015)]. From the field work, the length of the body, length of the long tail, and wingspan of the Tropicbird are known as 40 cm, 40 cm, and 96 cm. This work is finalized to implement the outer boundary shape of the Tropicbird so the length of the UAV is attained as 80 cm and the wingspan is attained as 96 cm. Based on these inputs, the other design parameters are estimated, which are overall weight, chord length, and tail, etc [James Louis Tangorra et al (2007)].

3.1 Design of UAV's Wing

Wing is the most important in UAV design. Wing plays a major role in lift production. Here the wing designs from the tropic bird which is the double tabard wing. And the location of the wing is High wing. A large size fixed wing is designed for high lift generation, so that the lift and buoyancy force overcomes the gravity force to make the UAV float [Gang Xue et al (2018)].

The wingspan of the UAV is taken from an adult tropic bird wing. In general, the Aspect Ratio (AR) of long-range UAV is should be more than 15 and medium velocity UAVs aspect ratios are varying 8 to 15. For this case the UAV works in medium velocity. As per the historical relation the aspect ratio was fixed. Using aspect ratio and wing span the wing area was estimated using following formula. From historical relation the wing loading was fixed and using those total weights is estimated.

$$S_{wing} = \frac{W_o}{W/_S} \text{ and } [\text{Aspect Ratio}]_{Wing} = \frac{b_{Wing}{}^2}{S_{wing}} \quad (1)$$

Likewise, from historical relation the taper ratio for forward and backward swept wing was estimated. Using known values and suitable formulae chord root, chord tip, swept angles, meaning aerodynamic chord and span wise chord are estimated. In general, the values Aspect Ratio (AR) of medium velocity based drones are lies between 8 and 15 so for this case AR is assumed as 10,

$$[\text{Aspect Ratio}]_{Wing} = \frac{b_{Wing}{}^2}{S_{wing}} \Rightarrow 10 = \frac{(96)^2}{S_{wing}} \Rightarrow S_{wing} = 921.6 \text{ cm}^2 \quad (2)$$

From the historical relationship, the value of the wing loading for this UAV is assumed as 0.0061793225 kg/cm^2.

$$S_{wing} = \frac{W_o}{W/_S} \Rightarrow W_o = [0.0061793225 \text{ kg/cm. square}] * 921.6 = 5.7 \text{ kg} \quad (3)$$

The wing consists of two parts, a rectangular wing that is forward swept wing and a tapered wing that is the backward swept wing. The forward swept wing helps to maintain the airflow over their surfaces at steeper climb angles than conventional plane. The swept back wings give the more lateral stability and less turbulence when speed abruptly changes. From the literature survey, it is found that 40% of wingspan is allocated for forward swept wing and 60% of the wingspan is allocated for backward swept wing. The half of the wingspan is equal to 48 cm, in which, 40% is allocated for first portion, which is 19.2 cm and 60% is collocated for second portion, which is 28.8 cm.

3.1.1 Design of forward swept wing

The relationship between Wingspan, chord length, and Wing Area,

$$S_{Wing} = b_{Wing} * C_{Wing-root} \quad (4)$$

$$C_{wing-root} = \frac{921.6}{96} = 9.6 \text{ cm}$$

From the Tropic Bird, the primary design details about first taper ratio is obtained, which slightly tilted forward swept wing.

$$\text{First Taper ratio } (\lambda) = \frac{C_t}{C_k} \Rightarrow C_{Wing-kink} = \lambda * C_{Wing-root} = 0.95 * 9.6 = 9.12 \text{ cm} \quad (5)$$

$$\text{Forward Sweep Angle} = \tan^{-1}\left(\frac{C_{wing-root} - C_{Wing-kink}}{\text{Wingspan of forward swept wing}}\right) \Rightarrow \tan^{-1}\left(\frac{9.6 - 9.12}{19.2}\right)$$

$$\text{Forward Sweep Angle} = \tan^{-1}\left(\frac{0.48}{19.2}\right) \Rightarrow \tan^{-1}(0.025) \Rightarrow 1.4321^{\circ}$$

3.1.2 Design of Backward Swept Wing

Form the literature survey, it is found that $\lambda = 0.4$ is more suitable to provide low drag with high lift at positive angle of attack, therefore in this work $\lambda = 0.4$ is used

$$\text{Second Taper ratio } (\lambda) = \frac{C_k}{C_r} \Rightarrow C_{Wing-tip} = \lambda * C_{Wing-kink} = 0.4 * 9.12 = 3.65 \text{ cm} \quad (6)$$

In this work, high wing configuration is planned so in order to calculate chord any span wise location, the b/2 is important. Mean Aerodynamic Chord,

$$MAC = \frac{2}{3} * C_{wing-kink} * \frac{1 + \lambda + \lambda^2}{1 + \lambda} \Rightarrow MAC = \frac{2}{3} * 9.12 * \frac{1 + 0.4 + 0.4 * 0.4}{1 + 0.4} \quad (7)$$

$$\overline{C_{Wing}} = \frac{2}{3} * 9.12 * \frac{1.56}{1.4} = 0.667 * 9.12 * 1.1143 = 6.78 \text{ cm}$$

'y' location of the MAC on each half of the wing is,

$$y_{MAC} = \frac{b}{6}\left(\frac{1 + 2 * \lambda}{1 + \lambda}\right) \Rightarrow y_{MAC} = \frac{96}{6}\left(\frac{1 + 2 * 0.4}{1 + 0.4}\right) \Rightarrow y_{MAC} = \frac{172.8}{8.4} = 12.343 \text{ cm} \quad (8)$$

Span wise chord estimations

$$\frac{C}{C_{Wing-kink}} = 1 - \left[2(1 - \lambda)\frac{y}{b}\right] \quad (9)$$

At 25% of span of both the side,

$$C_{25\%} = C_{Wing-kink}\left[1 - \left[2(1 - \lambda)\frac{y}{b}\right]\right] \Rightarrow C_{25\%} = 9.12\left[1 - \left[2(1 - 0.4)\frac{7.2}{[96]}\right]\right]$$

$$C_{25\%} = 8.3 \text{ cm}$$

At 50% of span of both the side,

$$C_{50\%} = C_{Wing-kink}\left[1 - \left[2(1 - \lambda)\frac{y}{b}\right]\right] \Rightarrow C_{50\%} = 9.12\left[1 - \left[2(1 - 0.4)\frac{14.4}{[96]}\right]\right]$$

$$C_{50\%} = 7.45 \text{ cm}$$

At 75% of span of both the side,

$$C_{75\%} = C_{Wing-kink}\left[1 - \left[2(1-\lambda)\frac{y}{b}\right]\right] \Rightarrow C_{75\%} = 9.12\left[1 - \left[2(1-0.4)\frac{21.6}{[96]}\right]\right]$$

$$C_{75\%} = 6.66 \text{ cm}$$

Where, b – wing span, λ – taper ratio, Wingspan (b) = 96 cm

$$\text{Backward Sweep Angle} = \tan^{-1}\left(\frac{C_{wing-root} - C_{Wing-tip}}{\text{Wingspan of backward swept wing}}\right) \quad (10)$$

$$\Rightarrow \tan^{-1}\left(\frac{9.6 - 3.84}{28.8}\right) \Rightarrow \tan^{-1}\left(\frac{5.76}{28.8}\right) \Rightarrow \tan^{-1}(0.2) \Rightarrow 11.31^{\circ}$$

3.2 Design of Fuselage

The outer body of this proposed UAV's captured from Tropic Bird so the design relationships are formed through previous relevant articles [3].

$$\frac{\text{Maximum Diameter of the UAV's Fuselage}}{\text{Overall Length of the UAV}} = 0.20 \quad (11)$$

$$\frac{\text{Maximum Diameter of the UAV's Fuselage}}{80} = 0.20$$

$$\text{Maximum Diameter of the UAV's Fuselage} = 0.20 * 80 = 16 \text{ cm}$$

$$\frac{\text{Minimum Diameter of the UAV's Fuselage}}{\text{Overall Length of the UAV}} = 0.07 \quad (12)$$

$$\frac{\text{Minimum Diameter of the UUV's Fuselage}}{80} = 0.07$$

$$\text{Minimum Diameter of the UUV's Fuselage} = 0.07 * 80 = 5.6 \text{ cm}$$

$$\frac{\text{Length Between Nose tip to first connecting point of wing and fuselage}}{\text{Overall Length of the UAV}} = 0.20 \quad (13)$$

$$\frac{\text{Length Between Nose tip to first connecting point of wing and fuselage}}{80} = 0.20$$

$$\text{Length Between Nose tip to first connecting point of wing and fuselage} = 0.20 * 80 = 16 \text{ cm}$$

3.3 Propulsive System Design

Thrust requirement by the single propeller in co-axial propulsive system, in which the maximum forward velocity is assumed as 10 m/s and minimum forward velocity is assumed as 5 m/s. Also the diameter of the propeller is picked as 1.8 inches.

$$T = 0.5 * \rho * \pi * r^2 * [(V_e)^2 - (V_o)^2] \Rightarrow 0.5 * 1025 * 3.14 * 0.02286^2[(5)^2 - (1)^2] \quad (14)$$

$$\text{Thrust at 5 m/s} = 20.184 \text{ N and Thrust at 10 m/s} = 83.25 \text{ N}$$

$$\text{Power} = \frac{1}{2} * T * v * \left[\left(\frac{T}{A * v^2 * {}^{\rho}/_{2}} + 1\right)^{\frac{1}{2}} + 1\right] \quad (15)$$

$$(T)\text{Static Thrust (oz)} = P\,(\text{in}) * D^3(\text{in}^3) * RPM^2 * 10^{-10} \quad (16)$$

Where T is static thrust in ounces, R is RPM of the propeller, D is the diameter of a propeller in inches, p is the pitch of propeller in inches

$$T = 4.392399 * 10^{-8} * RPM * \frac{(d^{3.5})}{\sqrt{pitch}} * [4.23333 * 10^{-4} * RPM * pitch - V_0] \quad (17)$$

$$\text{Main Rotor's Pitch} = \frac{\text{Induced Velocity in } \frac{\text{inch}}{\text{s}}}{\text{Revoution Per Second}} = \frac{\text{inch}/_{\text{s}}}{\text{revolutions}/_{\text{s}}} = \text{inch / revolution} \quad (18)$$

Propeller Pitch is estimated 1.831 inch with the help of above mentioned formulae.

3.3.1 Estimation of Pitch angle and Chord of the Propeller

The standard analytical formulae to design the UAV's propellers are listed in Equations (19), (20), and (21), in which pitch angle and chord length of the propellers are dealt. With the help of Equations (19), (20), and (21), the design parameters of UAV's propeller are designed and the design data are listed in Table 1.

$$\theta = \text{arctangent}\left(\frac{P}{2 * \pi * r}\right) \quad (19)$$

$$b = \frac{8 * \pi * m * r}{n * C_L} \quad (20)$$

$$b = \frac{8 * \pi * \left(\frac{\sin(\theta) * \left(\tan(\theta) - \frac{1}{1.2} * \tan(\theta)\right)}{\left(1 + \frac{1}{1.2} * \tan(\theta)\right)}\right) * r}{n * C_L} \quad (21)$$

Table 1. Calculated design data of four blade propeller

Sl. No	Location (inch)	Pitch angle (θ) (degree)	Chord length (inch)
1	0.09	72.84539141	0.110774471
2	0.18	58.31016376	0.15531337
3	0.27	47.19872965	0.165639432
4	0.36	39.00367722	0.161167439
5	0.45	32.93969617	0.151448919
6	0.54	28.36580212	0.140538929
7	0.63	24.83443814	0.1300025
8	0.72	22.04524768	0.120366764
9	0.81	19.79640341	0.111743044
10	0.9	17.9500491	0.104084566

3.3.2 Aerofoil Selection for Propeller

Aerofoil is the fundamental platform of propeller so that needs to be estimated through Reynolds Number, maximum velocity of UAV, and Coefficient of Lift. The just said predominant parameters were estimated with the help of literature survey [R Vijayanandh et al (2020)].

Table 2. Comprehensive drag analysis of various aerofoils

Aerofoil	Coefficient of Drag (C_D)	Aerofoil	Coefficient of Drag (C_D)	Aerofoil	Coefficient of Drag (C_D)
NACA 0012	0.025	NACA 6409	0.0185	NACA 2410	0.0178
NACA 2414	0.019	NACA 0024	0.029	NACA 2412	0.0180
NACA 2415	0.0195	NACA 2408	0.0175	NACA 22112	0.0201
NACA 25112	0.0275	NACA 23012	0.02	NACA 63A010	0.03
NACA 63012A	0.026	NACA 63-215	0.021		

The NACA 2408 aerofoil is selected as best than others based on low co-efficient of drag value. Thus, through the help of obtained design data, the conceptual designs of UAV and its propeller are modeled. The conceptual design of propeller is revealed in Figures 1 and 2, the conceptual design of advanced UAV is shown in Figures 3 and 4.

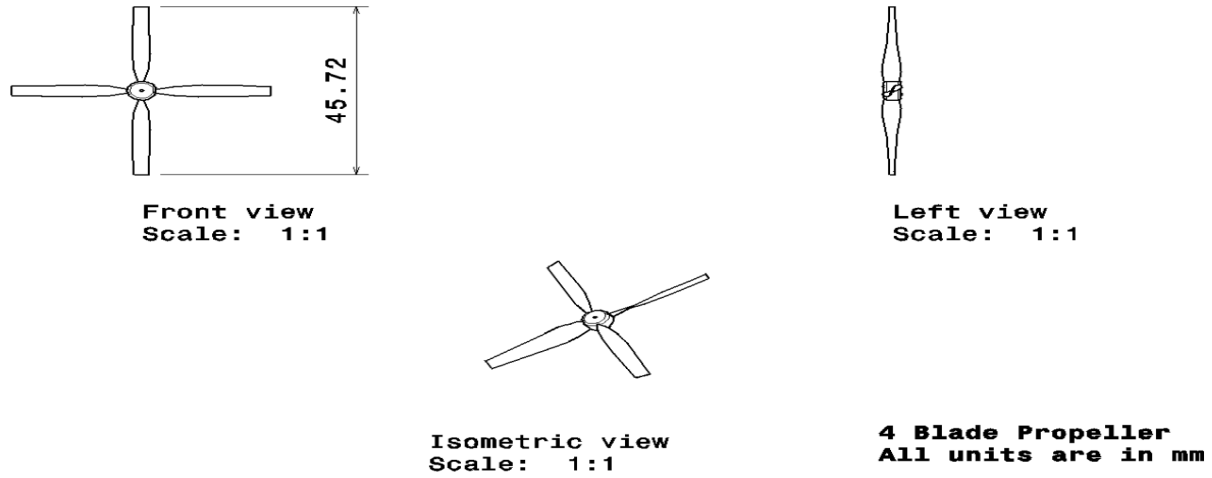

Figure 1. Design of selected UAV's Propeller

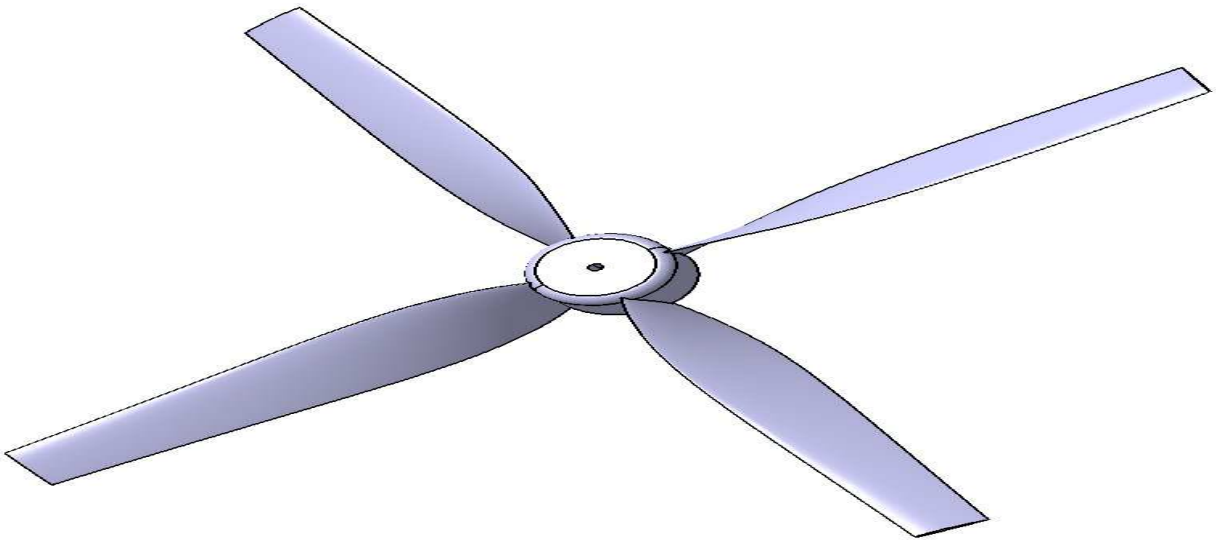

Figure 2. Conceptual Design of selected UAV's Propeller

The estimated values for wing dimensions are tabulated in Table 2.

Table 2. Final estimated data of UAV

S. No	Design description	Design data	S. No	Design description	Design data
1	Span	96 cm	10	Taper Ratio (FS)	0.95
2	Wing area	921.6 cm^2	11	Taper Ratio (BS)	0.4
3	Wing loading	0.0061793225 kg/cm^2	12	Swept angle (FS)	1.4321degree
4	Total weight	5.7 kg	13	Swept angle (BS)	11.31 degree
5	Span (forward swept)	19.2 cm	14	M.A.C	6.78 cm
6	Span(backward swept)	28.8 cm	15	Aspect ratio	14
7	Chord root (FS)	9.6 cm	16	Chord at 25% of span	8.3 cm
8	Chord tip (FS)	9.12 cm	17	Chord at 50% of span	7.45 cm
9	Chord tip (BS)	3.65 cm	18	Chord at 75% of span	6.66 cm

3.4 Design of UAV

Conceptual design of this advanced UAV is modeled with the help of CATIA. In the design, two-vertical stabilizers are fixed at the end of the wingtip in order to achieve easy maneuvering. Propeller is fixed at the end of the fuselage using connecting rod to prevent it from damaging. Since the propeller is in airfoil shape it creates considerable lift and controls buoyancy lift. The small size of the propeller withstands the hydrodynamic force imposed by the water. And for wing design, the respective sweep angle is made [Osman Md Amin et al (2017)].

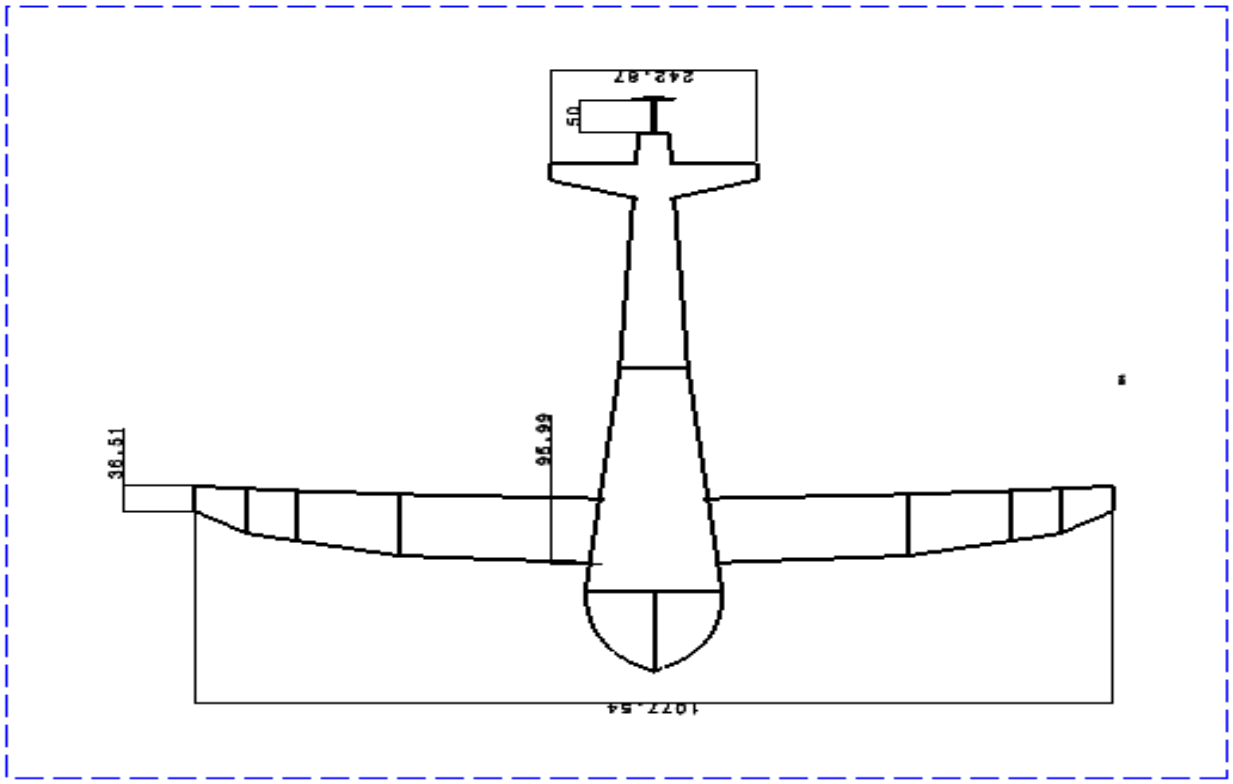

Figure 3. Design draft of the complete nature based UAV

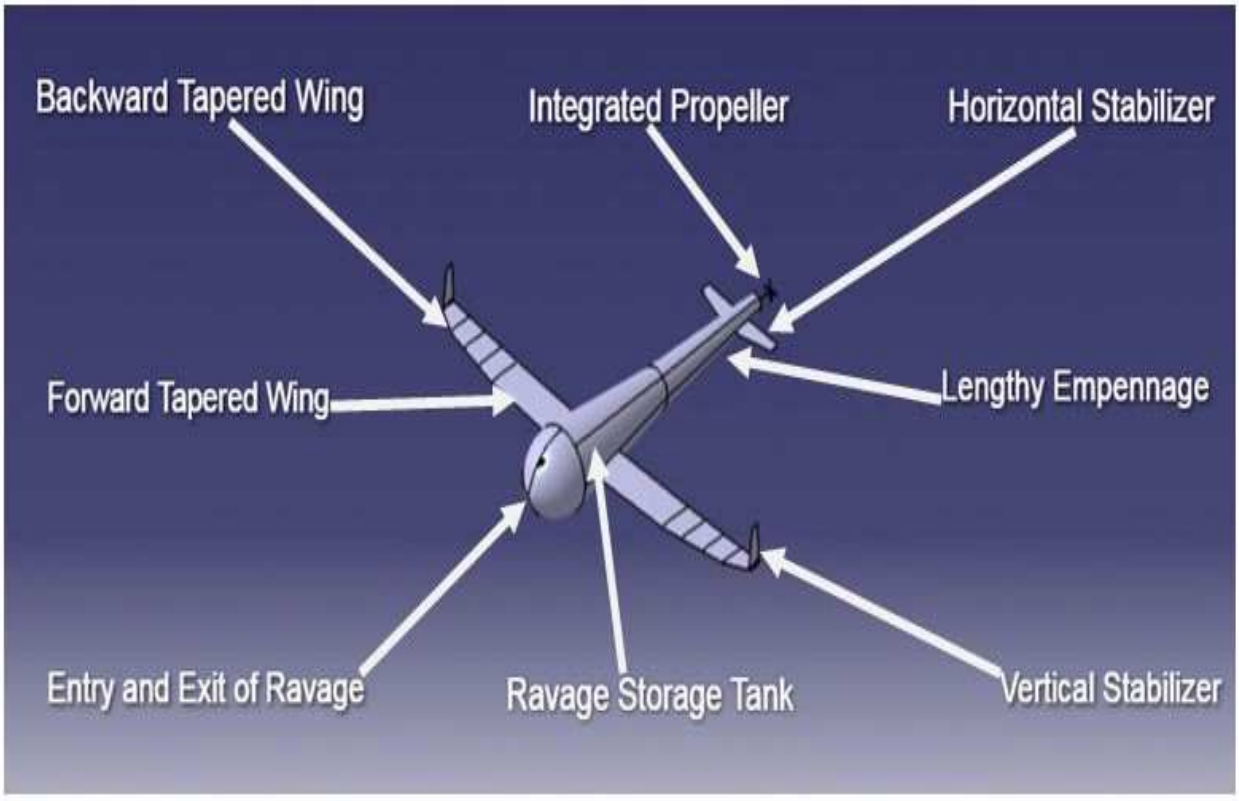

Figure 4. Conceptual design of nature inspired UAV

IV. PROPOSED METHODOLOGY – Advanced Computational Analysis

The proposed methodology for this work is advanced computational analysis, in which the various environments such as aerodynamic, aero-structural, hydrodynamic, and hydro-structural are solved with the help of ANSYS Fluent and structural tools. Fluid and structural dynamics are predominant computational analyses are imposed on UAV to investigate its different maneuvering conditions.

4.1 Computational Aerodynamic and Hydrodynamic Fluid Analyses

Fluid dynamic analysis provides a link between pressure, velocity and geometry of channels or closed volume through which flow is occurring. The two main purpose of fluid dynamic analysis is to find whether our UAV can overcome the drag force, so that the required RPM of propeller to be calculated and to analyze how much impact the fluid cause on the solid body of UAV. Cylinder shaped enclosure is taken to enclose the bodies of the model. The respective dimension for enclosure is 2.5m radius. The flow direction is "X" axis, so in the positive direction 2.5m and for negative direction 7.5m enclosure is created. The negative direction was longer than the positive because for analyze the flow after the UAV. Then, Boolean operation is done for subtracting the model from the enclosure because the nature of this analysis is external flow analysis. The updated control volume is discretized into small volumes, in which the compositional parts formed are nodes and elements. The type of mesh used for UAV was unstructured grid. Proximity and curvature are chosen for size function because the area varies of different location of UAV. Fine relevance center is used to get minute nodes and medium smoothening is used. Finally, the quantity of

mesh is attained minimum valued of 0.95 and maximum value of 0.9925. The wireframe model of the discretized structure is revealed in Figure 5.

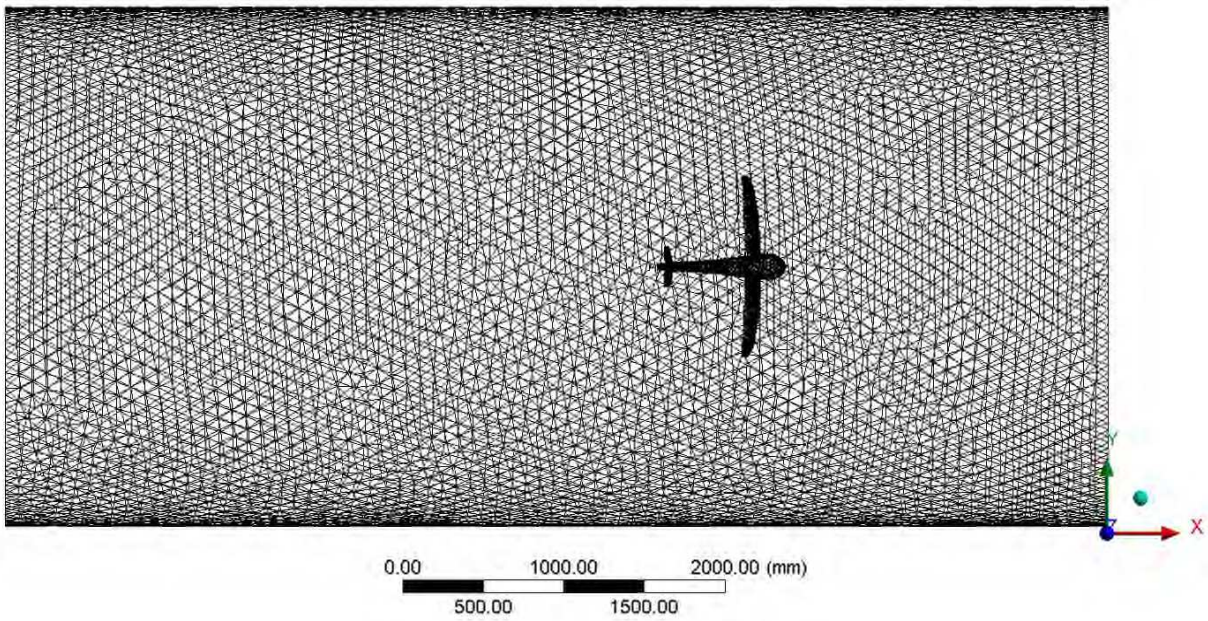

Figure 5. Discretization of computational model

After the discretization, the boundary conditions must be given for the UAV model. Because given boundary to a model can give the required result, which highly reliable in nature. Four boundaries are given to the computational model. In "X" direction inlet and outlet are given using named selection, and the subtracted part is given as UAV finally the rest of the parts have given as wall. For inlet, the hydro fluid velocity is given as 5m/s and the aero fluid velocity is given as 10 m/s. On outlet 0 gauge pressure is maintained for both the cases. For wall and UAV, no-slip and specified shear are given respectively. The solver is chosen as pressure based solver and the model used was k-epsilon to improve the results accuracy. Second order upwind also chosen in solution method in order to get accuracy of results. Material used is fluid with density of 1025 kg/m^3 for hydrodynamic computation and fluid density of 1.2256 kg/m^{3}is used for aerodynamic computation. Three major fluid dynamic computations are investigated, which are aerodynamic studies on UAV when it is flying above the ocean, aerodynamic cum hydrodynamic studies on UAV when it is flying on the ocean, and hydrodynamic studies on UAV when it is flying inside the ocean at the depth of 5m.

4.1.1 Grid Convergence Study – I

To pick the suitable grid, which can able to reliable outcome, the grid convergence test has been conducted on all kind of computational analyses. Therefore this comprehensive investigation executed two different grid independent tests, which are test on grid finalization for aerodynamic fluid computation and test on grid finalization for equivalent stress based hydro-structural computation. Figure 6 is revealed the comparative mesh outcomes of first grid convergence test and Figure 9 is shown the comparative mesh outcomes of second grid convergence test. Totally five different mesh cases are imposed for both the tests, wherein unstructured fine, unstructured fine

proximity, unstructured fine curvature, unstructured fine with adoptive mesh, and unstructured fine with inflation are the various five mesh cases used.

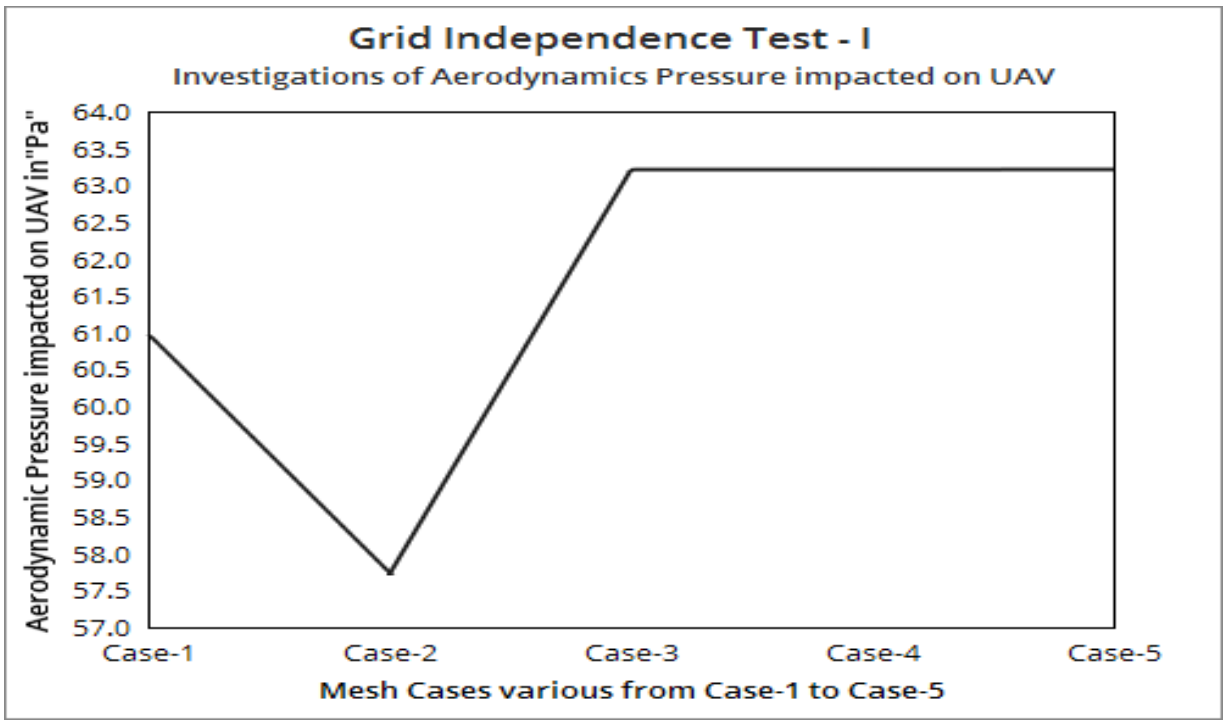

Figure 6. Grid Independence Test – I

4.2 Computational Aero-Structural and Hydro-Structural Analyses

The pressure of the fluid can deform or translate the structures which are interacted to them. The fluid also changes the structural and thermal stresses in the structures and thereby the flow pattern after the structure and induced velocity may also differ. So, the fluid - structural interaction [FSI] analysis is helps to study about those impacts. Another purpose of this proposed FSI analysis is to estimate the suitable material which can withstand the hydrodynamic impact load. Thus, the best lightweight material to resist the fluid loads for the UAV for all kind of oceanic working environments can be estimated. For FSI, the computational fundamental model is design of UAV. The deformation, equivalent stress, and normal stress over a UAV are the major outcome these FSI analyses. Computationally, meshing plays major role, which can help for better result and fast calculations. The type of mesh used for UAV is unstructured mesh because the complicated curvature design of UAV is directly linked with the generation of mesh. Proximity and curvature based mesh features are chosen for size function, owing to the variations of area of different location of UAV. The discretized structure of UAV for structural simulation is clearly revealed in Figure 7. After the discretization the boundary conditions are applied on the UAV. Fixed support is given at the end of the UAV and root face of the wing. Remote displacement is given for guide the deformation from a point on the hub region of integrated propeller and finally the pressure load is imported through one-way coupling approach based HSI simulation. The detailed given boundary conditions of this advanced UAV are revealed in Figure 8.

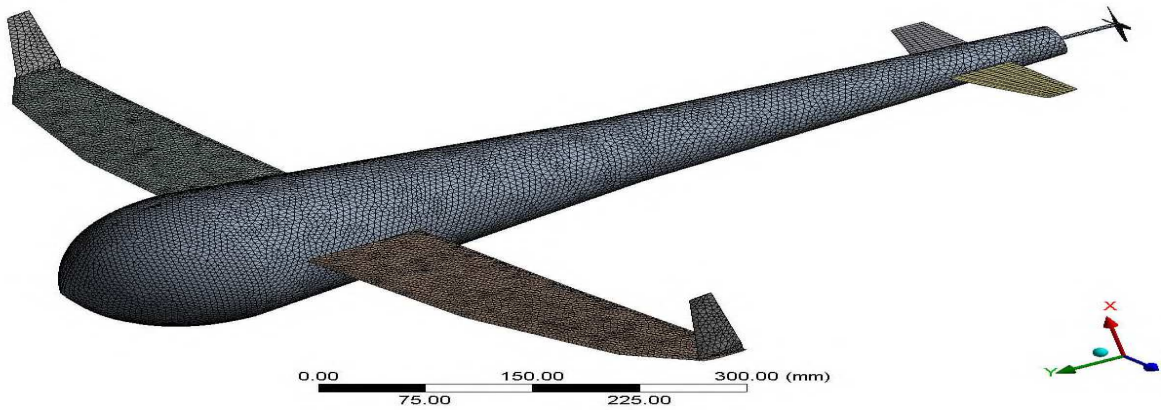

Figure 7. Meshed structure of UAV for HSI simulation

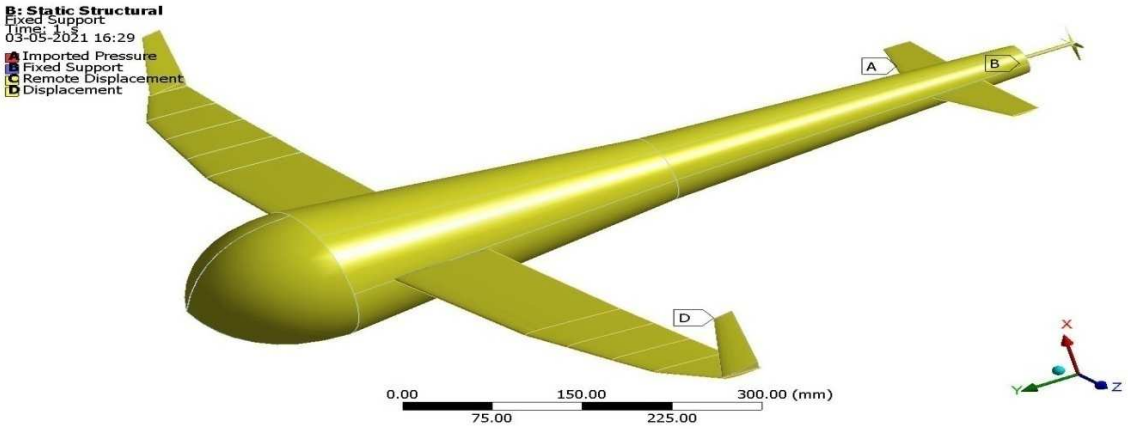

Figure 8. Boundary conditions imposed under FSI environment

4.2.1 Grid Convergence Study – II

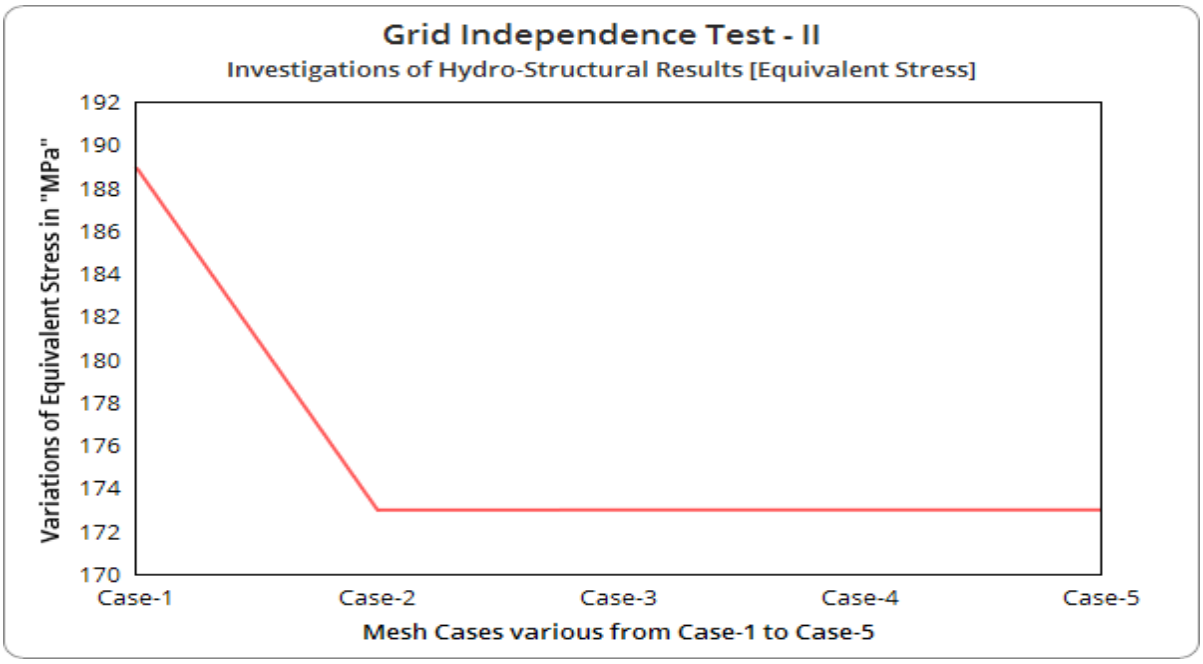

Figure 9. Grid Convergence Test – 2

From Figure 6, it is observed that mesh case – 3 is performed well than other cases based on low compositional elements and high reliable outcome production. The mesh case – 3 is unstructured fine curvature. From Figure 9, it is observed that mesh case – 2 is achieved greater than other mesh cases under equivalent stress based outcome of hydro-structural computation. The mesh case – 2 is unstructured fine proximity. Hence the same shortlisted mesh cases are extended for all the other simulations.

V. RESULTS AND DISCUSSIONS

The major outcomes composed and discussed in these comparative investigations are aero and hydrodynamic forces acted on UAV, aero and hydrodynamic pressure distributions on UAV, velocity variations over the UAV, structural deformation of UAV, and stresses induced in UAV structure. All of the just said outcomes are predominantly contributed in the selection of lightweight material for UAV and its overall efficiency. Totally, three different oceanic in and above environments are imposed these advanced computations, which are above the ocean surface, on the ocean surface, and inside the ocean. The computational aerodynamic simulation is computed for above the surface of ocean, the computational hydrodynamic simulation is computed for inside the ocean, finally the combined simulation is computed for on the surface of the ocean. Figures 10 to 12 are revealed the results of above the ocean surface and thereby the comprehensive results of the same conditions are revealed in Figures 13 to 16. Figures 17 to 19 are revealed the results of above the ocean surface and thereby the comprehensive results of the same conditions are revealed in Figures 20 to 25.Figures 28, 29, and 32 are revealed the results of above the ocean surface and thereby the comprehensive results of the same conditions are revealed in Figures 33 and 34.

5.1 CFD Results – Above the surface of Oceans

The aerodynamic flow velocity of 10 m/s based computational results is shown in Figures 10 to 12. In Figure 10, the negative sign of pressure is corresponds for dynamic pressure and the velocity induced by the shape of the UAV is 2.414 m/s [Vijayanandh R et al (2020) and Vijayakumar Mathaiyan et al (2011)].

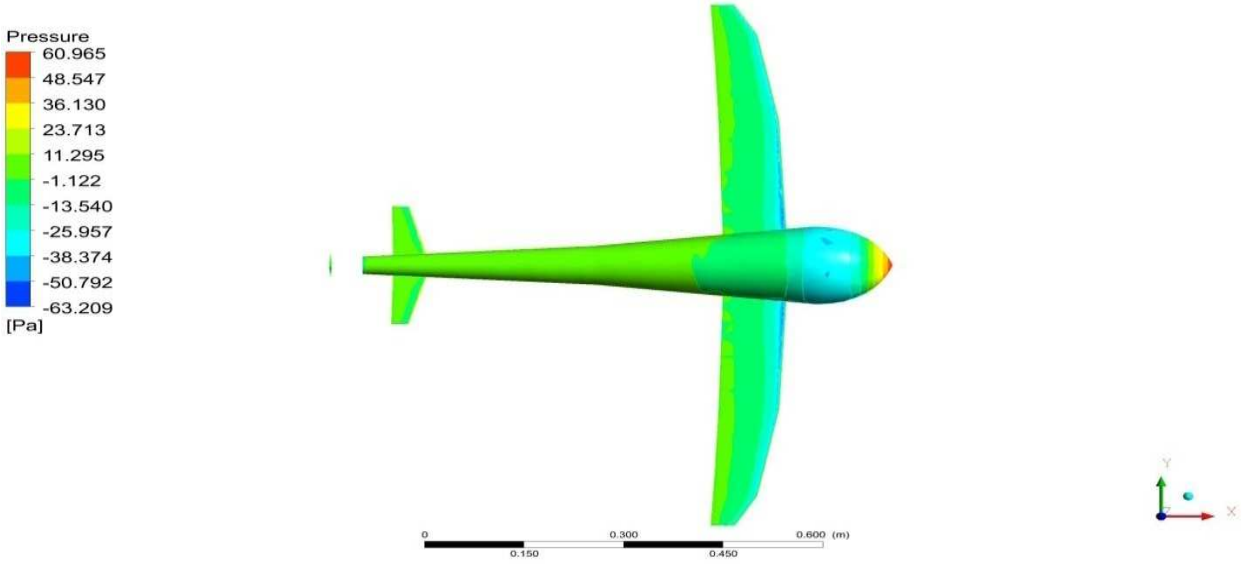

Figure 10. Aerodynamic Pressure variations on UAV when flying above the ocean

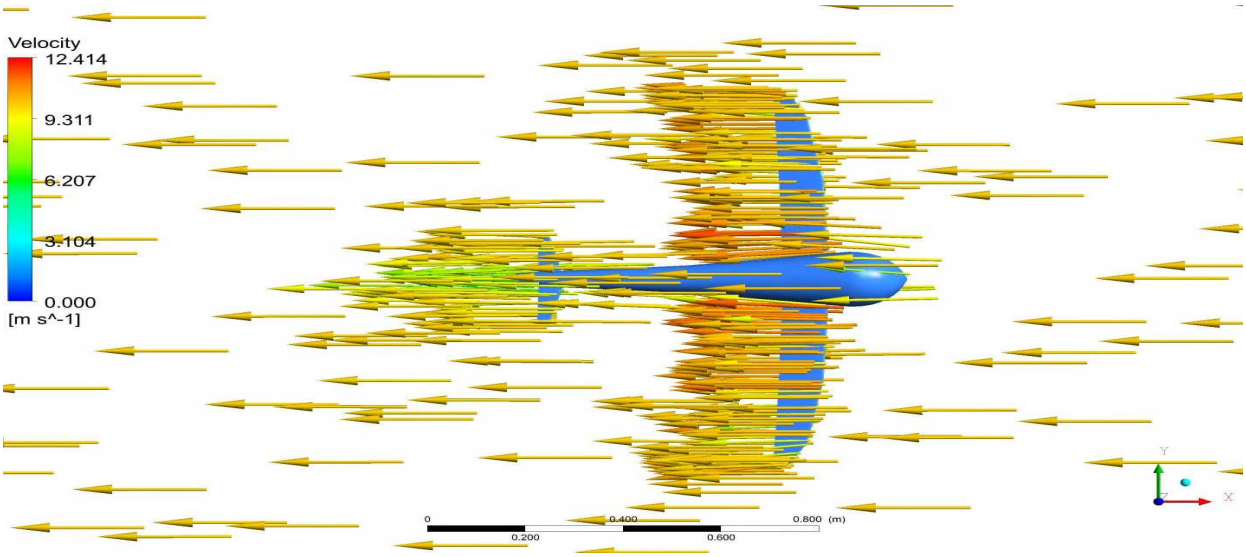

Figure 11. Velocity generation over the UAV when flying above the ocean

5.2 HSI Results – Above the surface of Oceans

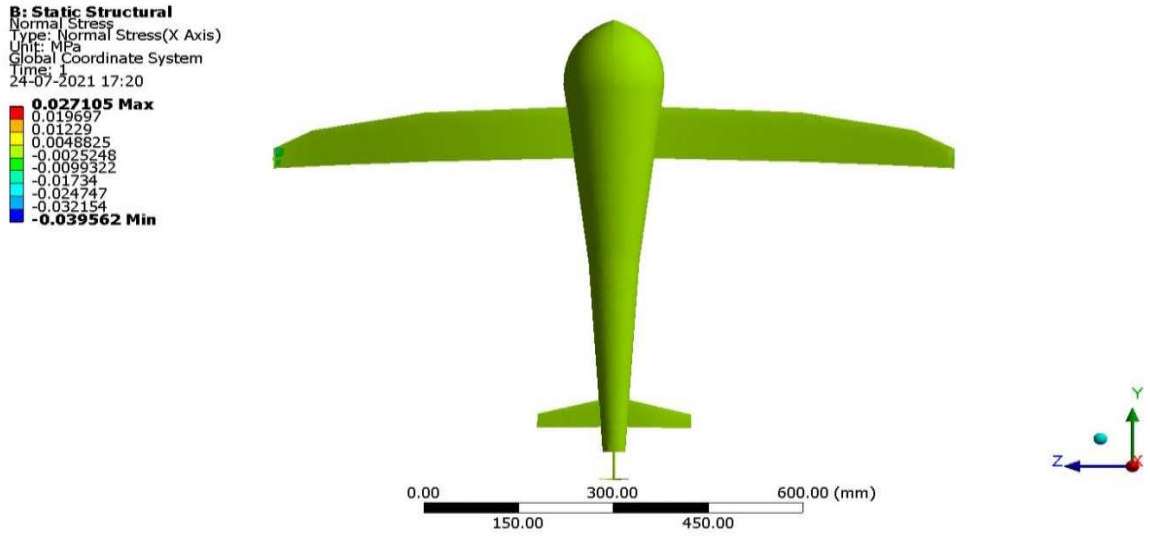

Figure 12. Stress induced in UAV – Manoeuvring at above the ocean

The normal stress induced in UAV under the imposing of GFRP [Glass Fiber Reinforced Polymer]-W-FR4 based composite is revealed in Figure 12. Apart from this material, various other lightweight materials are also imposed FSI simulations, in which the implemented materials are Aluminum Alloy, Stainless Steel, Grey Cast Iron, Magnesium Alloy, Polyethylene, Copper Alloy, Ti-Alloy, CFRP [Carbon Fiber Reinforced Polymer]-UD-Prepreg, CFRP-UD-Wet, CFRP-Woven-Prepreg, CFRP-Woven-Wet, E-Glass-UD, E-Glass-Wet, FR-4-Glass-Woven, S-Glass-UD, KFRP [Kevlar Fiber Reinforced Polymer]-49-UD. The best seven advanced alloys are picked and imposed for both of the aerodynamic and hydrodynamic impacted structural computations. Similarly, under the composite material category, the nine better lightweight materials are imposed above said FSI simulations. The selection factors involved in this work for suitability of lightweight material to resist both aerodynamic and hydrodynamic loads are low reactance of deformation and low induction of stresses.

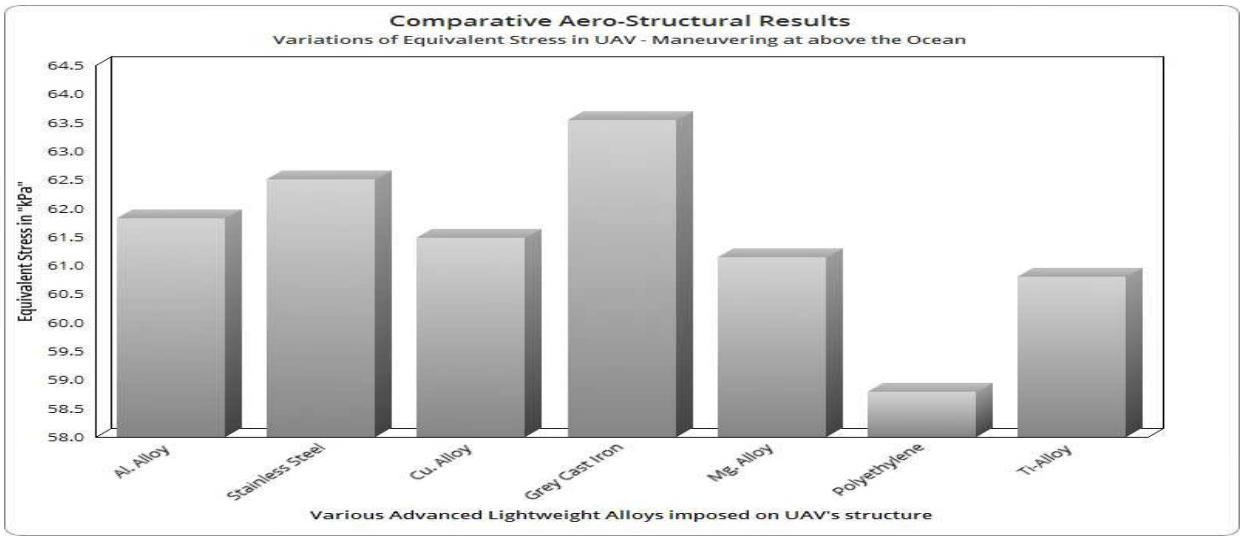

Figure 13. Comparative Equivalent Stress Variations for various alloys

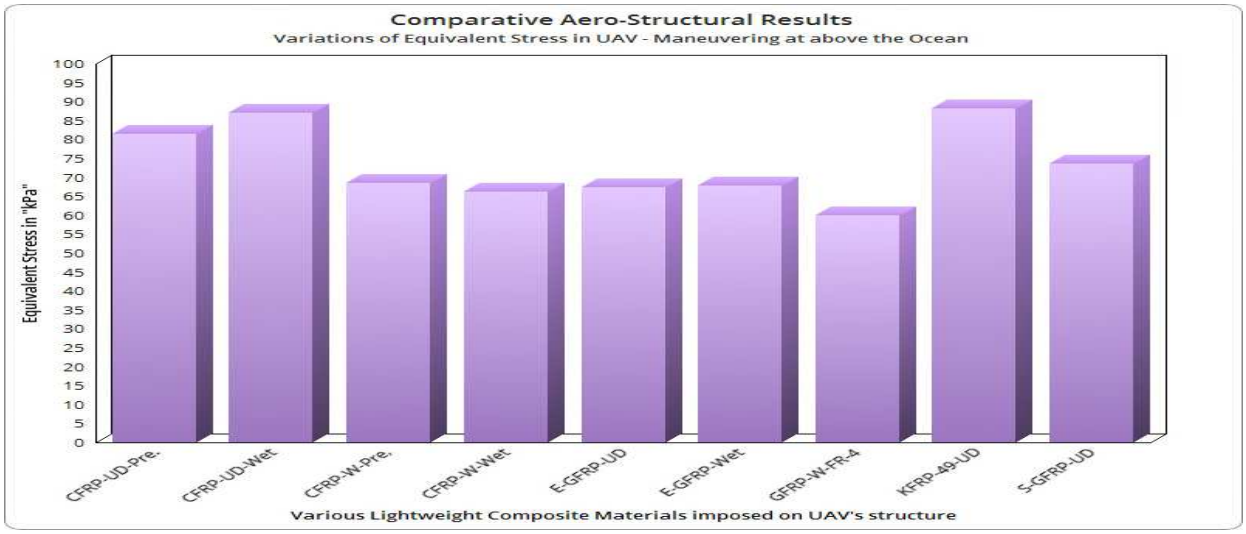

Figure 14. Comparative Equivalent Stress Variations for various composites

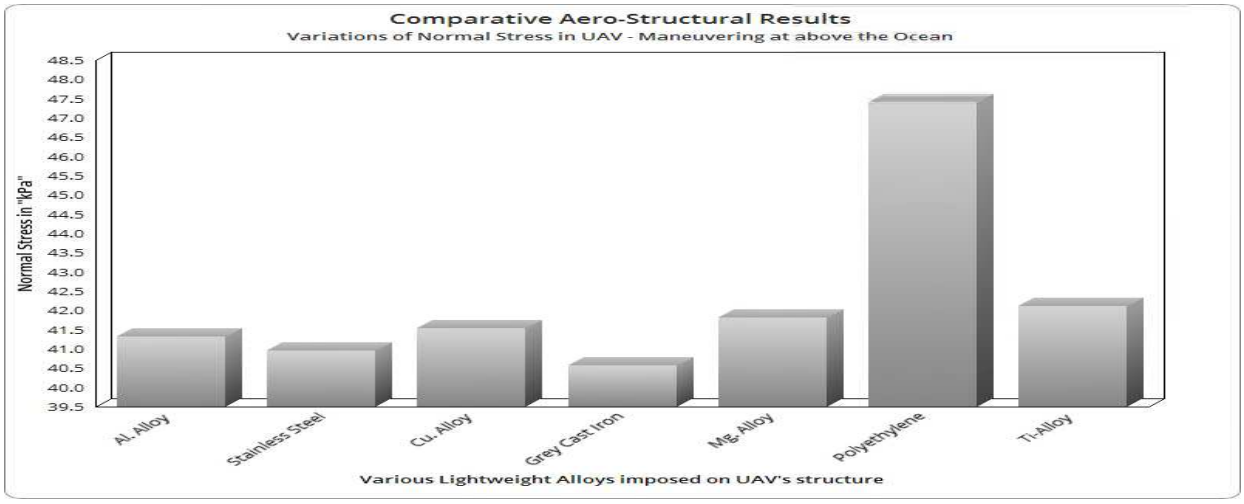

Figure 15. Comparative Normal stress variations for various alloys

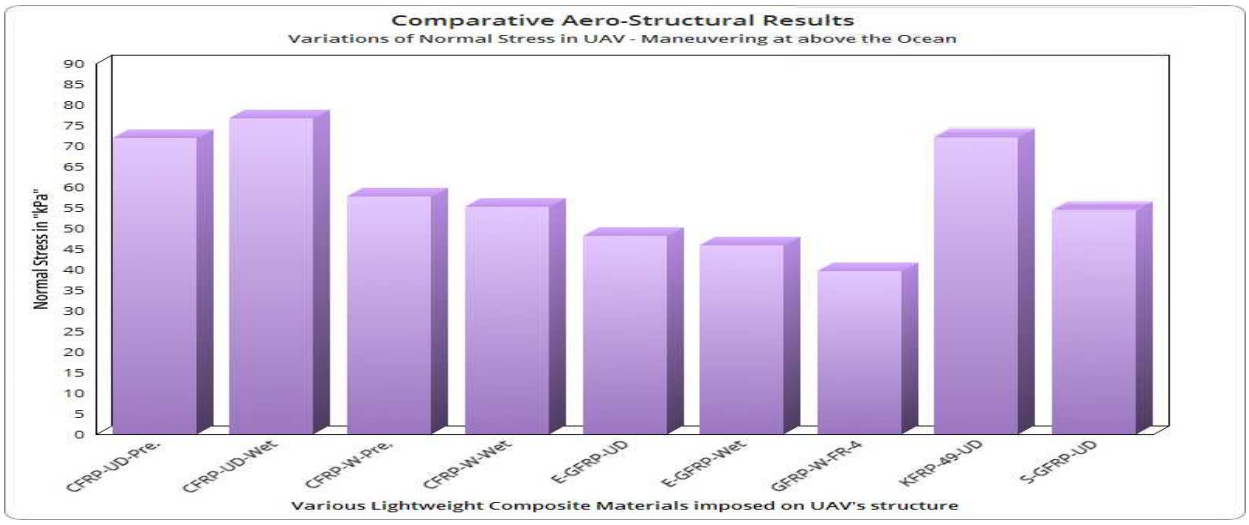

Figure 16. Comparative Normal stress variations for various composites

Equivalent stress and total deformations of various lightweight materials comprehensively represented in Figures 13 to 16. From Figures 13 to 16, it is strongly observed that GFRP [Glass Fiber Reinforced Polymer]-W-FR4 based composite is reacted lower than other lightweight materials under aerodynamic load. Thus, the lifetime of this same GFRP composite is quite higher than other lightweight material.

5.3 CFD Results – On surface of the Oceans

Using ANSYS Fluent, the hydrodynamic cum aerodynamic forces of UAV when it is maneuvering on the surface of the ocean are computed and the pressure load on the UAV, velocity flow over the UAV are estimated for 0.1m depth under the water. The maximum pressure on the UAV is obtained as 15000.900 Pa and the minimum of pressure is predicted as 1254 Pa. The pressure variations on UAV are clearly expressed in Figure 17.

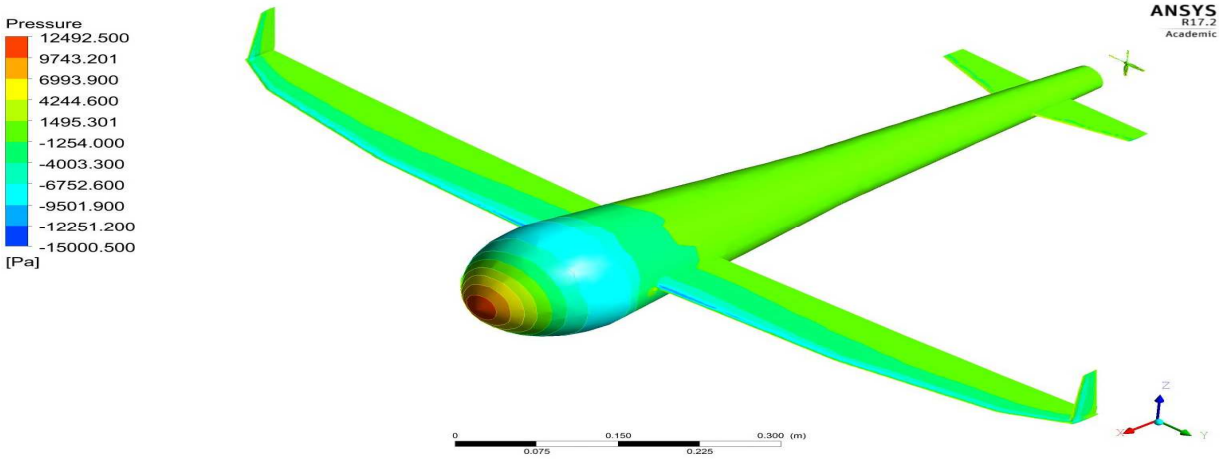

Figure 17. Hydrodynamic pressure distributions on UAV

The velocity flow over a UAV is apparently same on different location. The different view of velocity over the UAV is shown in Figure 18. The input velocity on the surface is measured and given as 5 m/s and thereby the induced velocity increased by 1.334 m/s [V Praveen Kumar et al (2019)].

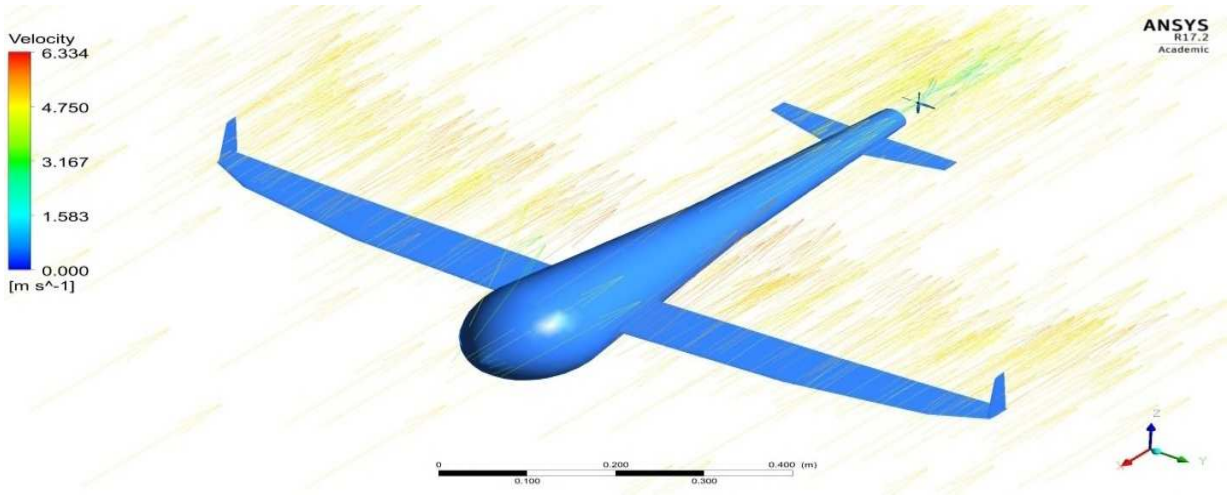

Figure 18. Velocity variations over the UAV

The hydrodynamic forces of Lift, Drag and Side forces are 66.9098 N, 37.2441 N and 0.180857 N respectively. The lift force is little higher than required amount. Reason for that is the span of the wing. Then the drag force is acceptable. Using that value, the rpm of propeller fixed. Because then only it can overcome that drag force. Additionally, the side force also estimated for general purpose.

5.4 FSI Results – On surface of the Oceans

As per the aerodynamic based FSI simulation, the same sixteen lightweight materials are chosen for this hydrodynamic analysis. The pressure load which is estimated at0.1 m depth is given as input to the structural simulation. For each material, equivalent-elastic strain, equivalent stress, normal stress, elastic strain and total deformation values are estimated using ANSYS structural tool. Based on the low reactance of structural outcomes, the best material is picked to resist for this environmental condition.

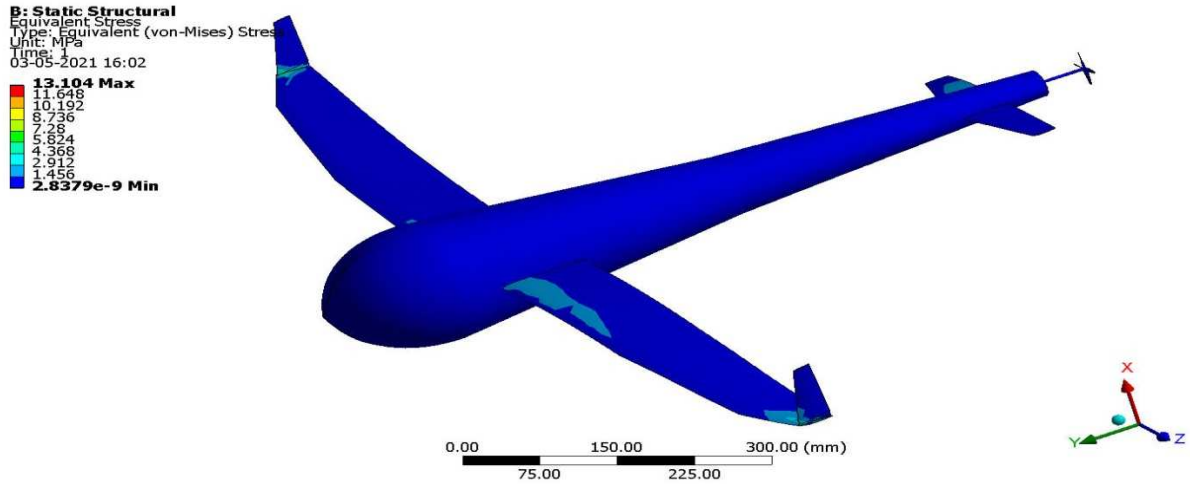

Figure 19. Variations of Equivalent Stress of GFRP-FR-4-Woven

The comprehensive results of this condition are revealed in Figures 20 to 25, wherein the total deformation, equivalent stress, and normal stress are focally considered as selection parameters.

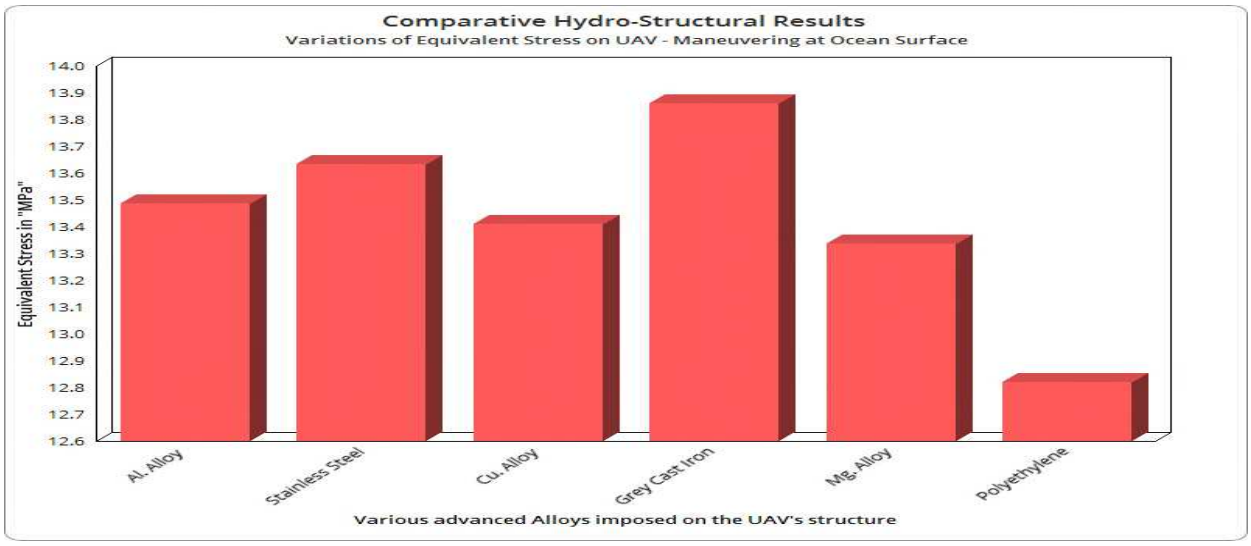

Figure 20. Comparative equivalent stress variations for various alloys

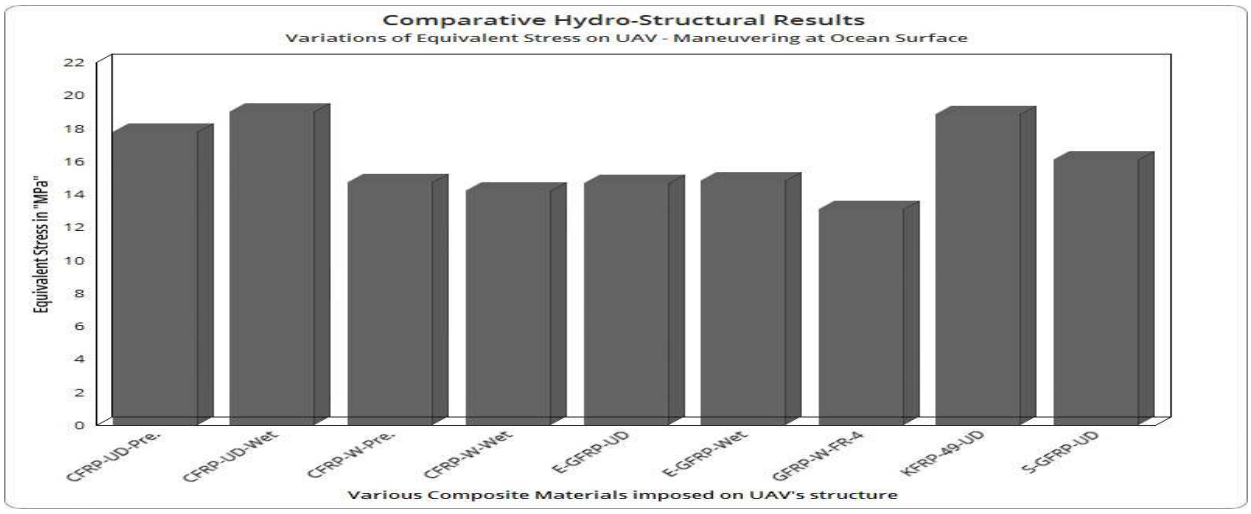

Figure 21. Comparative equivalent stress variations for various composites

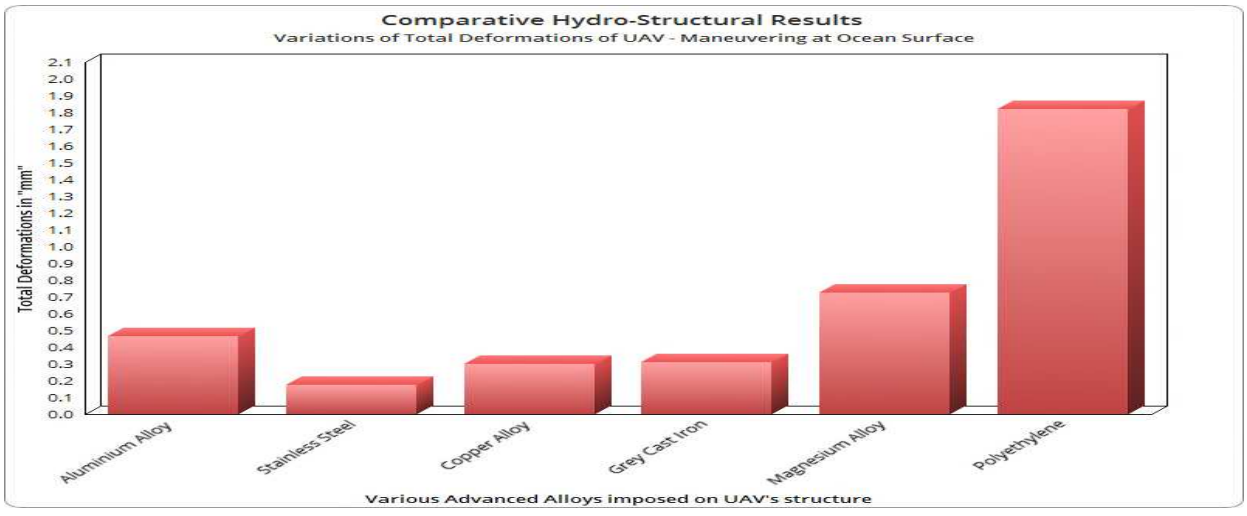

Figure 22. Variations of total deformations of different alloys

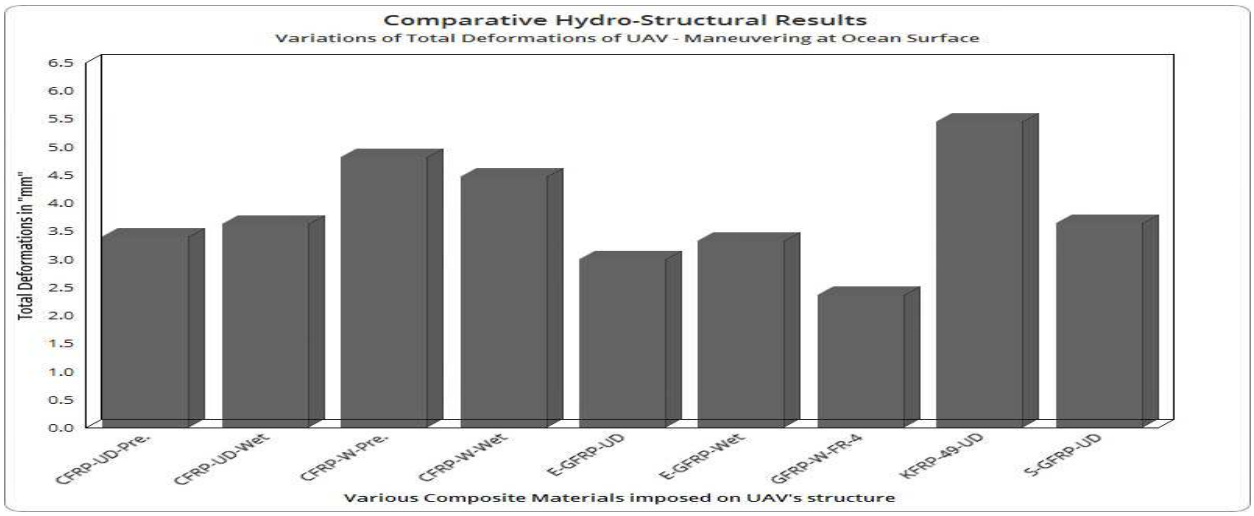

476

477 **Figure 23.** Variations of total deformations of different composite materials

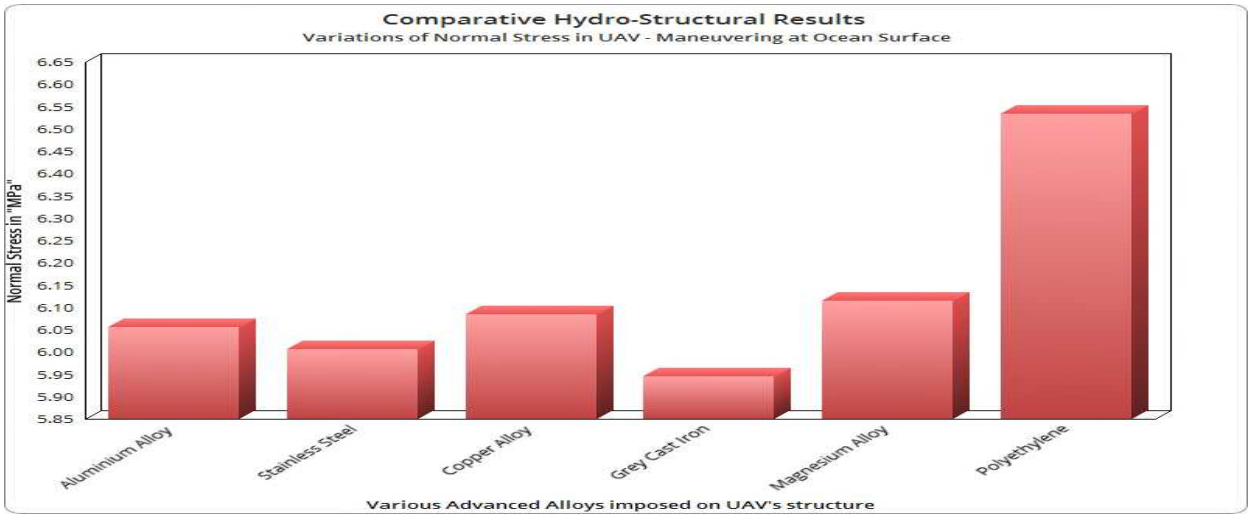

478

479 **Figure 24.** Comparative normal stress variations for various alloys

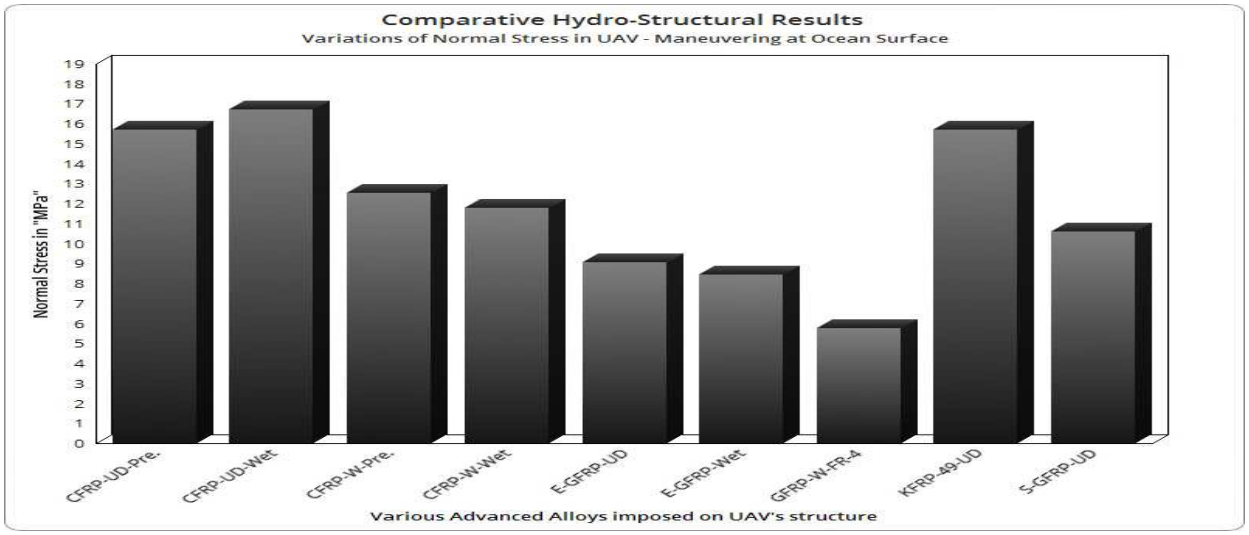

480

481 **Figure 25.** Comparative normal stress variations for various composites

In this the aluminum alloy and stainless steel are already existing material. With the reference of those two other materials deformations values are compared. Grey cast iron has less equivalent-elastic strain value (0.00013542). Likewise, Polyethylene has less equivalent stress (12.821), FR-4-Glass-woven has less normal stress (5.7784), Copper alloy has less elastic strain (0.007857), and at the end of the comparison the Copper alloy had the less deformation value (0.29923). The deformation of material is more important so that Copper alloy has selected for UAV under alloy category. From Figures 20 to 25, it is strongly observed that GFRP [Glass Fiber Reinforced Polymer]-W-FR4 based composite is reacted lower than other lightweight materials under both hydrodynamic and aerodynamic loads. Thus, the lifetime of this same GFRP composite is quite higher than other lightweight material.

5.5 Final Optimized Design and its CFD Results – Inside the Oceans

Due to the high lift generation, the foldable wing is proposed for this advanced UAV. Thus, another part of foldable wing is implemented in this condition, which is rectangular wing based on symmetrical aerofoil. The optimized cum flexible wing system supported UAV is modeled and revealed in Figures 26 and 27.

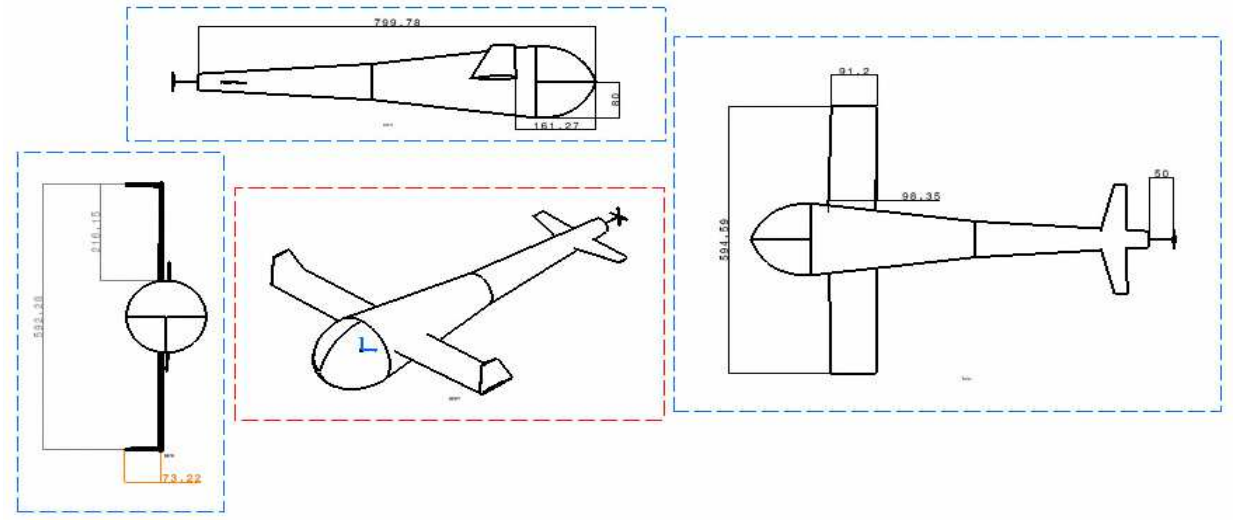

Figure 26. Design of optimized UAV

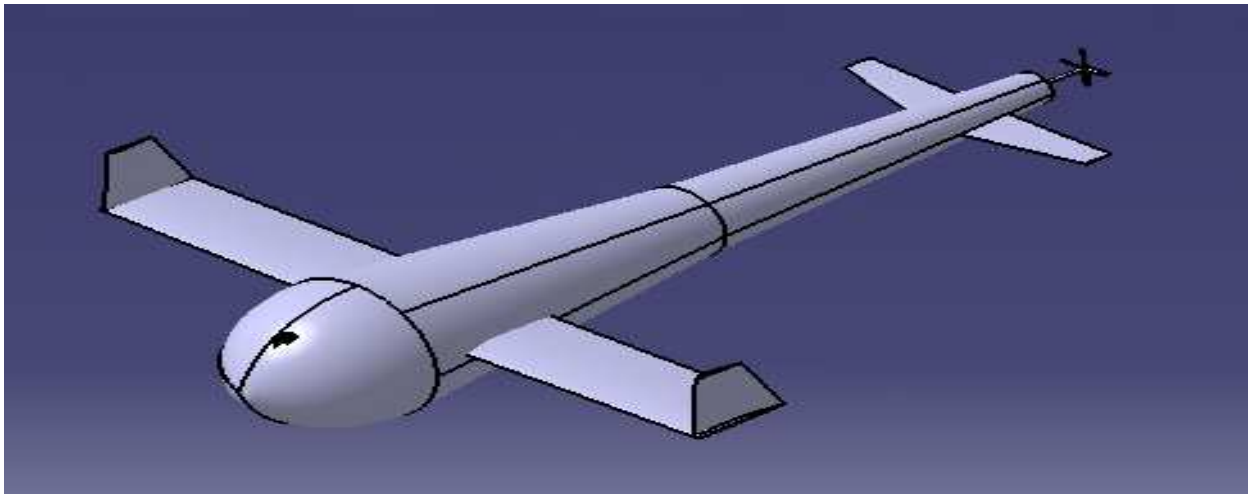

Figure 27. Conceptual design of optimized UAV

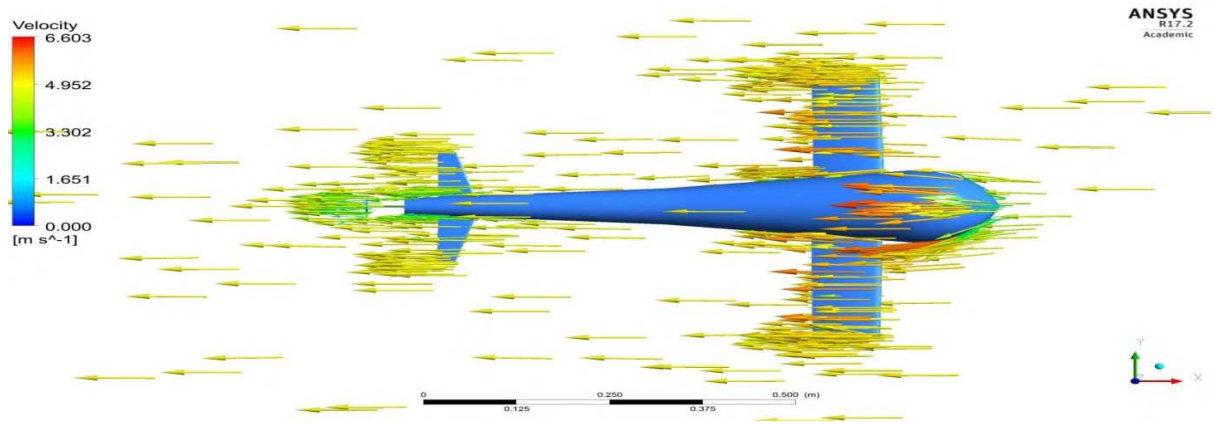

Figure 28. Hydrodynamic velocity generation over the optimized UAV

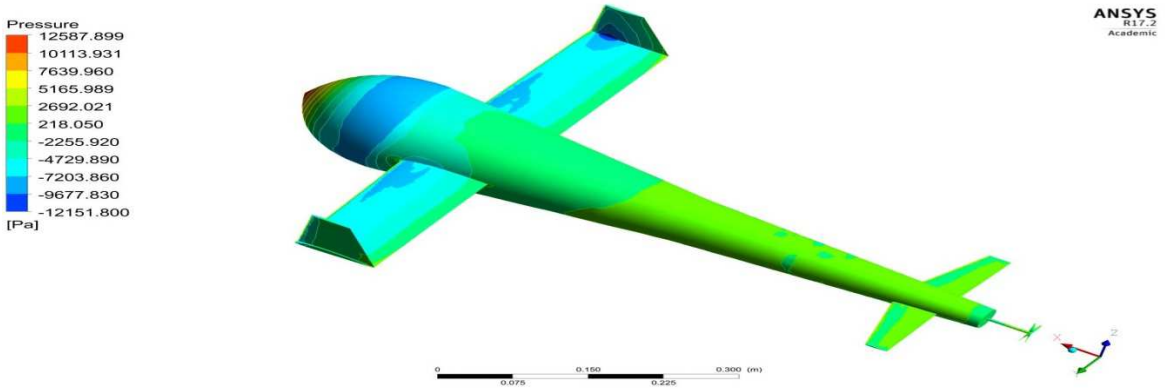

Figure 29. Hydrodynamic Pressure variations of optimized UAV

Figures 28 and 29 are shown the hydrodynamic velocity and pressure variations over the optimized UAV. The working environment picked for this condition is 5 m and the input velocity is assumed as 5 m/s. To clean maximum amount of unwanted ravages from the oceans, the surface of the ocean to 5 m depth inside the ocean is planned through this UAV. Therefore this computation is mandatory and the hydrodynamic forces of Lift, Drag and Side forces are estimated as172.796 N, 37.6144 N and 0.541549 N respectively.

5.6 Final Optimized Design and its HSI Results – Inside the Oceans

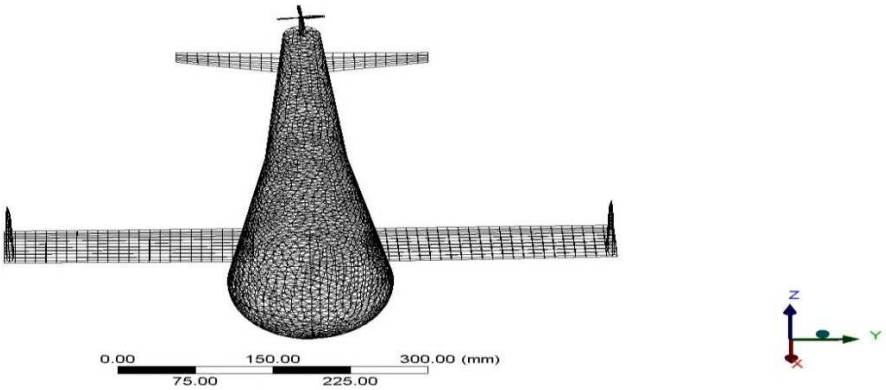

Figure 30. Discretized structure of optimized UAV

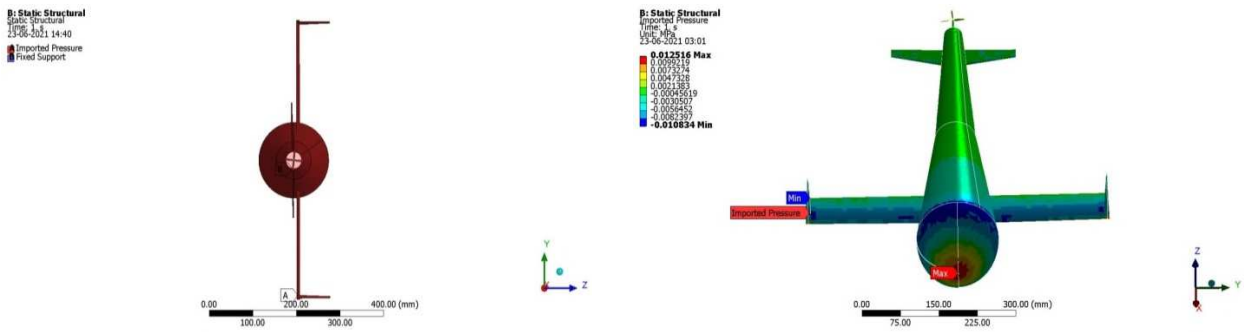

Figure 31. Boundary conditions imposed in optimized UAV

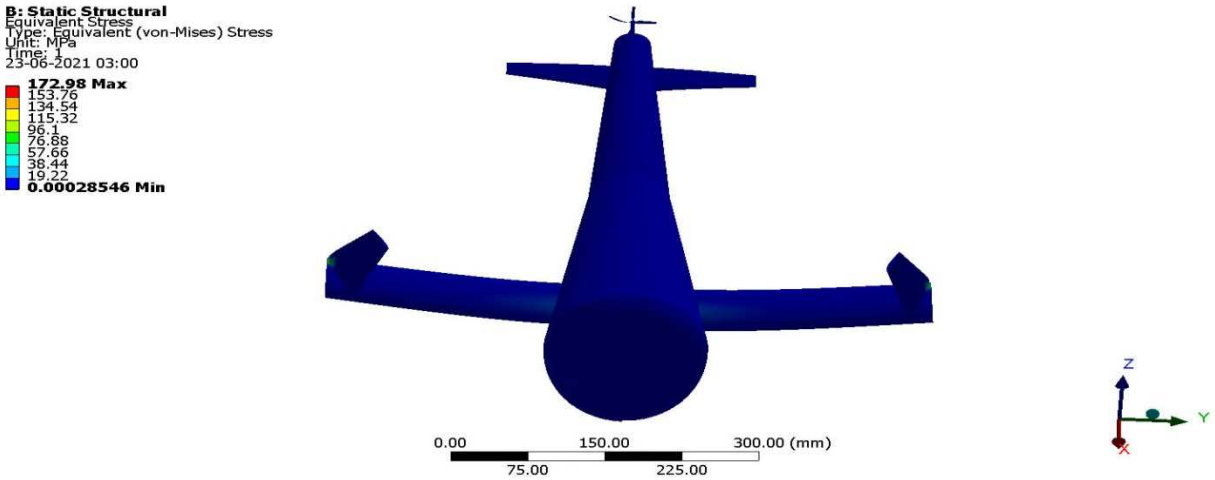

Figure 32. Equivalent Stress of GFRP-W-FR-4 based optimized UAV

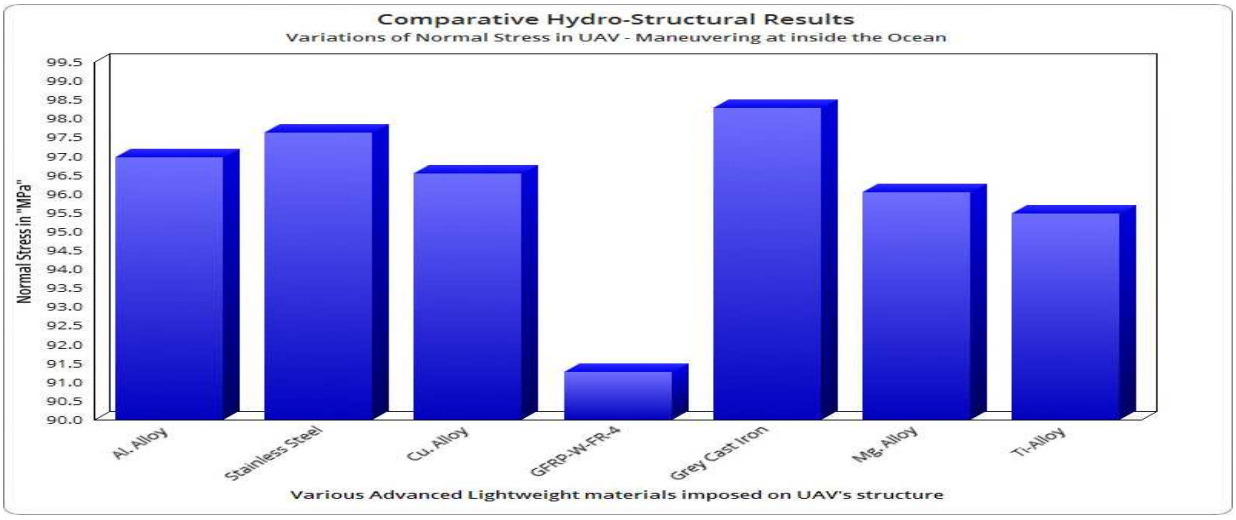

Figure 33. Comparative normal stress variations for various lightweight materials

The HSI results on this condition are computed and thereby the relevant outcomes are revealed in Figures 30 to 34. Figure 30 is revealed the unstructured feature based discretized structure of an optimized UAV. Apart from discretization, the boundary condition plays the focal role, which is shown in Figure 31, wherein imposed hydrodynamic pressure and fixed support are mentioned clearly. From first two investigations, GFRP composite and

all the alloys are performed better than other lightweight materials, so the best seven lightweight materials are underwent this complicated HSI simulation. The comprehensive results of normal and equivalent stresses are clearly shown in Figures 33 and 34.

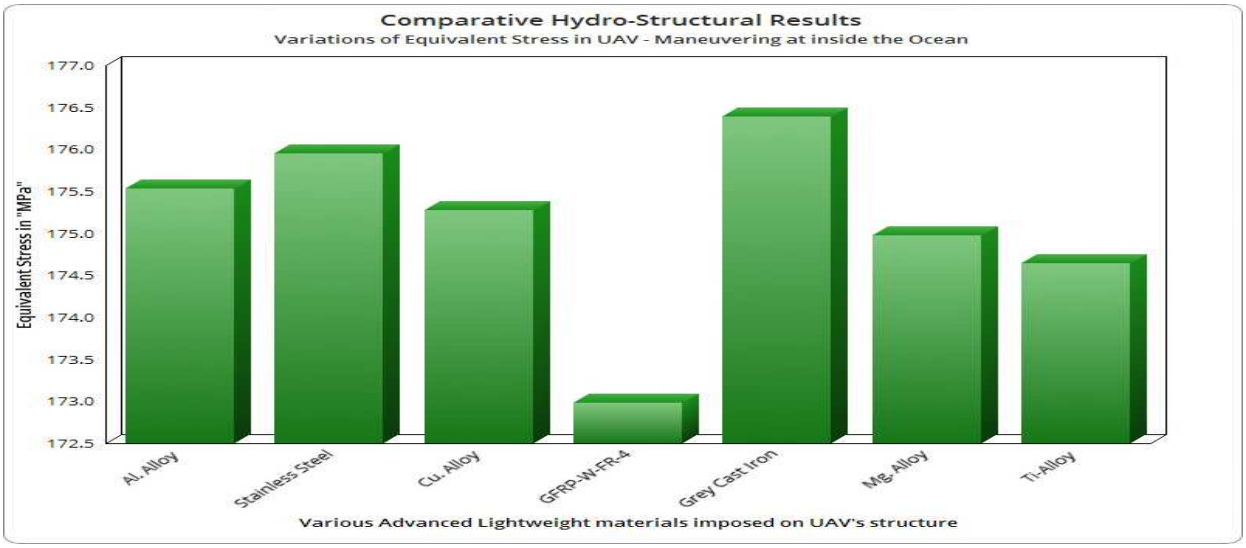

Figure 34. Comparative equivalent stress variations for various lightweight materials

From Figures 33 and 34, it is strongly noted that GFRP-W-FR4 based composite is reacted lower than other lightweight materials under both hydrodynamic load. Thus, the lifetime of this same GFRP composite is quite higher than other lightweight material. So, GFRP-Woven-FR4 based lightweight composite is perfect to implement in the structure of UAV because it can able withstand both aerodynamic and hydrodynamic loads.

VI. RAVAGE ISSUE AND ITS REMOVAL APPLICATION

The ravage focused in this work is the debris/waste that forms on the surface of the water and submerged to some extent under the water. The debris/waste includes all forms of plastic waste, sewage waste, oil spills etc. Oil spills are liquid petroleum hydrocarbon released into the ocean/water bodies by manmade disasters, drilling rigs, offshore platforms etc. The leakage of oil spills in the ocean is a form of pollution especially marine. These oil spills have adverse effect on marine ecosystem in such a way that it forms the blocking coat over the surface of the water. This blockade does not allow the oxygen to dissolve in and out of the water. This in turn causes the marine species suffer from insufficient dissolved oxygen, thus causing the death of living marine organisms. These oil spills not only affect the fishes in the marine ecosystem but also affects the birds and other mammals. That is, the oil spill penetrates into the anatomical structure of the plumage of the birds and the fur of other mammals. Due to this penetration, they lose their insulating ability. This in turn will make them vulnerable to more temperature fluctuations. This will also make them denser and so they become less buoyant. These oil spills will bring adverse effects for the society. Unfortunately, the fact is that cleaning the oil spills is a difficult task and it depends on many factors such as the type of oil that is spilled, the water temperature, the type shoreline, the type of beaches/ocean involved etc. Cleaning the oil spills physically is so expensive. The method of bioremediation using bacteria is a better method, but only to some extent, since abundant bacteria is needed and also this method requires the external

factor to support. The Seabin project can also be a possible solution but that is the static model. Similar to these techniques fewer advances have made to clean up the oil spills but that was not cost efficient. By considering all these factors an idea come up with a solution of having a dynamic movable model, which is capable of locating the debris and also clean up such spills. The dynamic movable model is the UAV which proves to be the possible solution in the near future [Mike Eichhorn et al (2018)].

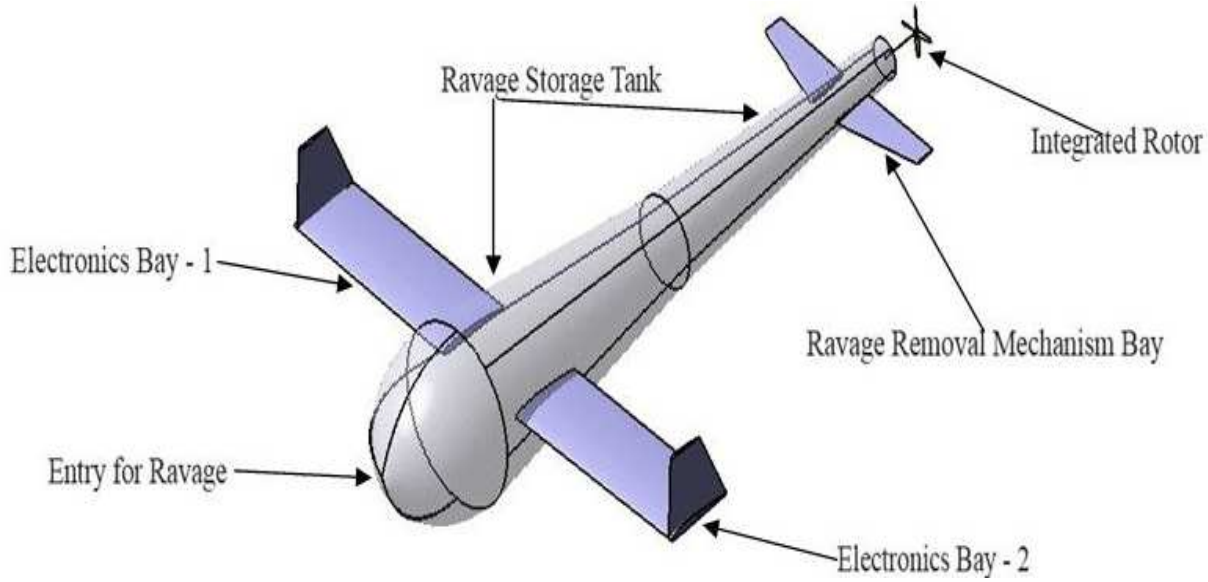

Figure 35. Components and arrangements of UAV at the stage of collection of ravage

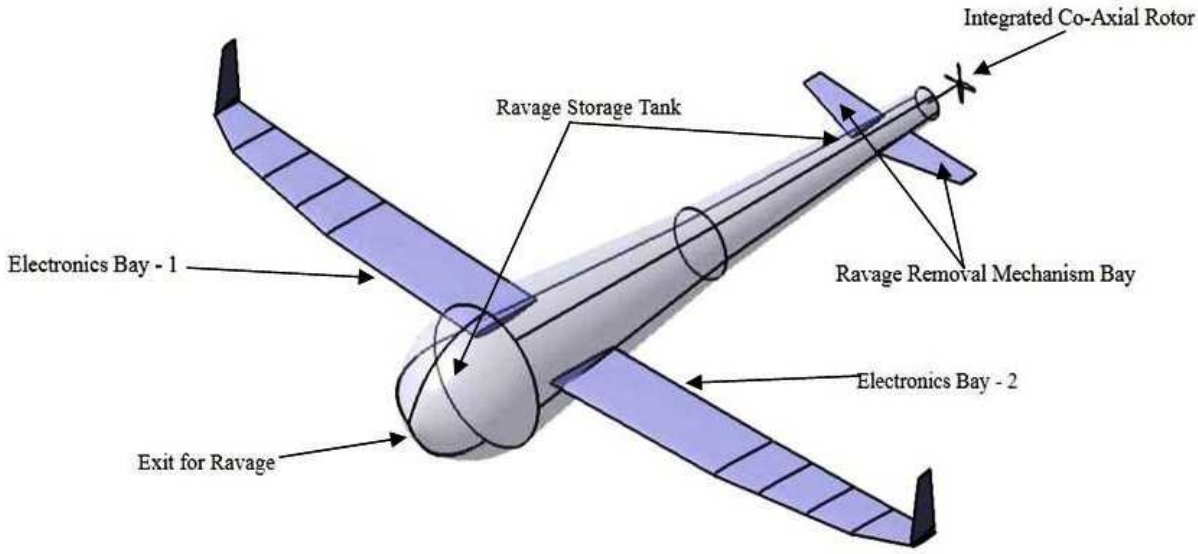

Figure 36. Components and arrangements of UAV at the stage of removal of ravage

The collection and removal ravage system based UAV phases and its corresponding components are revealed in Figures 35 and 36. Through the help of three different environmental conditions based multi-disciplinary investigations, the proposed dynamic model of UAV based ravage collector is constructed perfectly with inclusion of all the major conclusions from the abovementioned three comparative investigations. The constructed dynamic ravage collector UAV is ready for the deployment.

VII. CONCLUSIONS

The paper work encloses the conceptual design of flexible and efficient UAV. Bio-inspired species of this UAV has the high stability to withstand conditions on and under the water. Since the tropic bird can fly with high stability and high maneuvering capacity, the bio-inspired UAV can implement the mission without any disturbances and execute the sudden altitude variations with payload. Once the conceptual design of the UAV is modeled with the help of CATIA, the aerodynamic and hydrodynamic forces are estimated using ANSYS Fluent. The drag forces are monitored clearly and the same forces are indented to design and select the suitable propulsive system for this highly maneuverable UAV. The velocity flows over a UAV at various working oceanic environments are apparently the same and linear in different locations because of this proposed UAV's design. Therefore the drag is generated is quite lower than other conventional UAV models. Additionally, the FSI analyses are computed on UAV at two different working environments [above and on the ocean surfaces] under the counts of sixteen lightweight materials and thereby the suitable materials are picked to withstand such mentioned conditions. Common observation is alloys are good to withstand complicated fluid loads and GFRP-Woven-FR4 based composite material is overall best performer. Then, the next FSI analysis is carried out on UAV under the Ocean at the depth of 5 m and so the suitable material is picked to resist such kind of environment. At last, it is strongly Overall the required UAV has been conceptually modeled to meet the ravage removal application. One major observation is found that GFRP-Woven-FR4 based composite material is best lightweight material to resist all kinds of oceanic environments thus the same material is strongly suggested for the implementation in UAV's real time application. The designed UAV is capable of providing good conditions for the cleaning mechanism to take place. Bio-inspired structure of the UAV when modeled gives extraordinary support for the ravage removal. This will set the base for the inventions in ravage removal.

Declarations

Ethics approval and consent to participate

Not applicable

Consent for publication

Not applicable

Availability of data and materials

Not applicable

Competing interests

The authors declare that they have no competing interests

Funding

There is no any external and internal funding sources are available for this manuscript

Authors' contributions

SKM – SKM is the main author to finalize this innovation approach on UAV and did Literature Survey.

VR – Proposed Methodology and its computations are computed by VR

SG – Conceptual Design of first UAV was modeled by SG

DKM – Conceptual Design of second UAV was modeled by DKM

APR – Literature Survey and manuscript preparation were did by APR

DKJ – Manuscript preparations were did by DKJ

Acknowledgements

Computational facilities are been provided by the authors' parent institution, which is Kumaraguru College of Technology, Coimbatore, Tamil Nadu, India. So, all the authors of this article would like to thank all the management of people and higher professionals.

REFERENCES

Agus Budiyono (2009) Advances in unmanned underwater vehicles technologies: Modeling, control and guidance perspectives. Indian Journal of Marine Sciences 38: 3 282 – 295.

Chenhui Han et al (2019) Reversible Switching of the Amphiphilicity of Organic-Inorganic Hybrids by Adsorption–Desorption Manipulation. The Journal of Physical Chemistry 123: 34 21097–21102. DOI: 10.1021/acs.jpcc.9b07040.

Daniele Costa et al (2018) Design of a Bio-Inspired Autonomous Underwater Robot. J Intell Robot Syst, 91:181–192. https://doi.org/10.1007/s10846-017-0678-3

Dylan K Wainwright et al (2020) Tunas as a high-performance fish platform for inspiring the next generation of autonomous underwater vehicles. Bioinspiration & Biomimetics 15: 3. https://doi.org/10.1088/1748-3190/ab75f7.

Gang Xue et al (2018) Motion Model of Fish-like Underwater Vehicle and its Effect on Hydrodynamic. IEEE Xplore 978-1-5386-1078-7/18:1-5. DOI: 10.1109/ISMA.2018.8330134

James Louis Tangorra et al (2007) The Development of a Biologically Inspired Propulsor for Unmanned Underwater Vehicles. IEEE Journal of oceanic engineering 32: 3 533 – 550. DOI: 10.1109/JOE.2007.903362.

Joon-Young Kim et al (2011) Dynamic Modeling and Structural Analysis of Manta-Type UAV, 25: 31 4319–4322. DOI:10.1142/S0217979211066866.

Meliha Bozkurttas et al (2008) Understanding the Hydrodynamics of Swimming: From Fish Fins to Flexible Propulsors for Autonomous Underwater Vehicles, Advances in Science and Technology, 58, 193-202, doi:10.4028/www.scientific.net/AST.58.193

Mike Eichhorn et al (2018) Modular AUV Integrated Real-Time Water Quality Analysis. Sensors 18: 6 1837. doi: 10.3390/s18061837.

Negrello, F et al (2016) Preliminary design of a small-sized flapping UAV: II. Kinematic and structural aspects. Meccanica 51: 6, 1369–1385. https://doi.org/10.1007/s11012-015-0309-7

Osman Md Amin et al (2017) Development of a highly maneuverable unmanned underwater vehicle on the basis of quad-copter dynamics. AIP Conference Proceedings 1919, 020009. https://doi.org/10.1063/1.5018527

R Vijayanandh et al (2020) Theoretical and Numerical Analyses on Propulsive Efficiency of Unmanned Aquatic Vehicle's Propeller. IOP Journal of Physics: Conference Series 1504: 012004 1-10. https://doi.org/10.1088/1742-6596/1504/1/012004

Tae-Hwan Joung et al (2006) A Study on the Structural Design and Analysis of a Deep-sea Unmanned Underwater Vehicle. J. Ocean Eng. Technol. 20: 3 7-14.

Vijayakumar Mathaiyan et al (2011) Conceptual Design and Numerical analysis of an Unmanned Amphibious Vehicle, AIAA Scitech 2021 Forum, 2021, https://doi.org/10.2514/6.2021-1285.

Vijayanandh R et al (2020) Conceptual Design and Comparative CFD Analyses on Unmanned Amphibious Vehicle for Crack Detection, Unmanned Aerial System in Geomatics, Lecture Notes in Civil Engineering, eBook ISBN: 978-3-030-7393-1, 14, pp. 133-150, 2020, https://doi.org/10.1007/978-3-030-37393-1_14

V Praveen Kumar et al (2019)Conceptual Design And Hydrodynamic Research On Unmanned Aquatic Vehicle, International Journal of Innovative Technology and Exploring Engineering, ISSN: 2278-3075, Volume-8, Issue-11S, pp 121 – 127, 2019, DOI: 10.35940/ijitee.K1027.09811S19.

Xiao-xu DU et al (2014) Analysis of hydrodynamic characteristics of unmanned underwater vehicle moving close to the sea bottom, Defence technology 10:1 76-81. https://doi.org/10.1016/j.dt.2014.01.007

Yung-Lien Wang, Chung-Hui Tai & Hung-Ru Huang (2015) Design and development of an autonomous underwater vehicle – robot dolphin, Journal of Marine Engineering & Technology, 14:1, 44-55. DOI: 10.1080/20464177.2015.1022383